Potential field methods in delineating architectural settings of the Eastern Yilgarn Craton (EYC)

Indrajit G. Roy, Richard Lane, Richard Blewett and Paul Henson
*pmd*CRC c/o Geoscience Australia GPO Box 378, Canberra ACT 2601 Australia.*

Introduction

The Eastern Yilgarn Craton (EYC) is a part of greater Archaean Yilgarn Craton and it hosts major orogenic gold deposits (Morey et al., 2007; Hagemann and Cassidy, 2000; Eisenlohr et al., 1989). The science philosophy of the *pmd*CRC* has been to consider a the mineral system in terms of five questions, *viz: (1) geodynamics, (2) architecture, (3) fluid sources and reservoirs, (4) fluid pathways and drivers, and (5) depositional mechanisms* (Barnicoat, 2007). A comprehensive understanding to these questions requires the integration across various geoscience disciplines (such as geology, geochemistry, geophysics, numerical modelling etc.). For example, to delineate architectural framework at the subsurface, geophysical methods/data (such as deep seismic, gravity and magnetic etc.) play important roles and hence those methods with ensuing interpretation techniques have been aptly used in this research project.

The studied area in this report is ranging from 120˚E - 124˚37'E and 25˚S - 33˚S, covering an area approximately 404,514 km^2 of EYC. However, for the sake of convenience and for detailed studies at some zones of interest we have divided the entire area in several sub-domains. Figure 1 show the entire studied area and some sub-domains within it, where detailed studies have been carried out.

Here we give an account of the techniques of data processing and modelling of potential field (Gravity and Magnetic) data and their applications to delineate architectural settings of the studied area. We use deep seismic data sparingly for interpretation as availability of deep seismic data has been limited within the studied area. Discussion of seismic data processing and modelling is beyond the scope of the present report. However, we outline the processing details of regional gravity and magnetic data sets, involving grid transformations, image processing enhancements, multi-scale edge detection (“worming”), and default-parameter (“unconstrained”) 3D inversion, forward gravity and magnetic modelling to generate 2D sections, determining depth to the magnetic basement etc. In our potential field data processing and modelling we use Bouguer gravity, airborne magnetic and topographic data in the studied area.

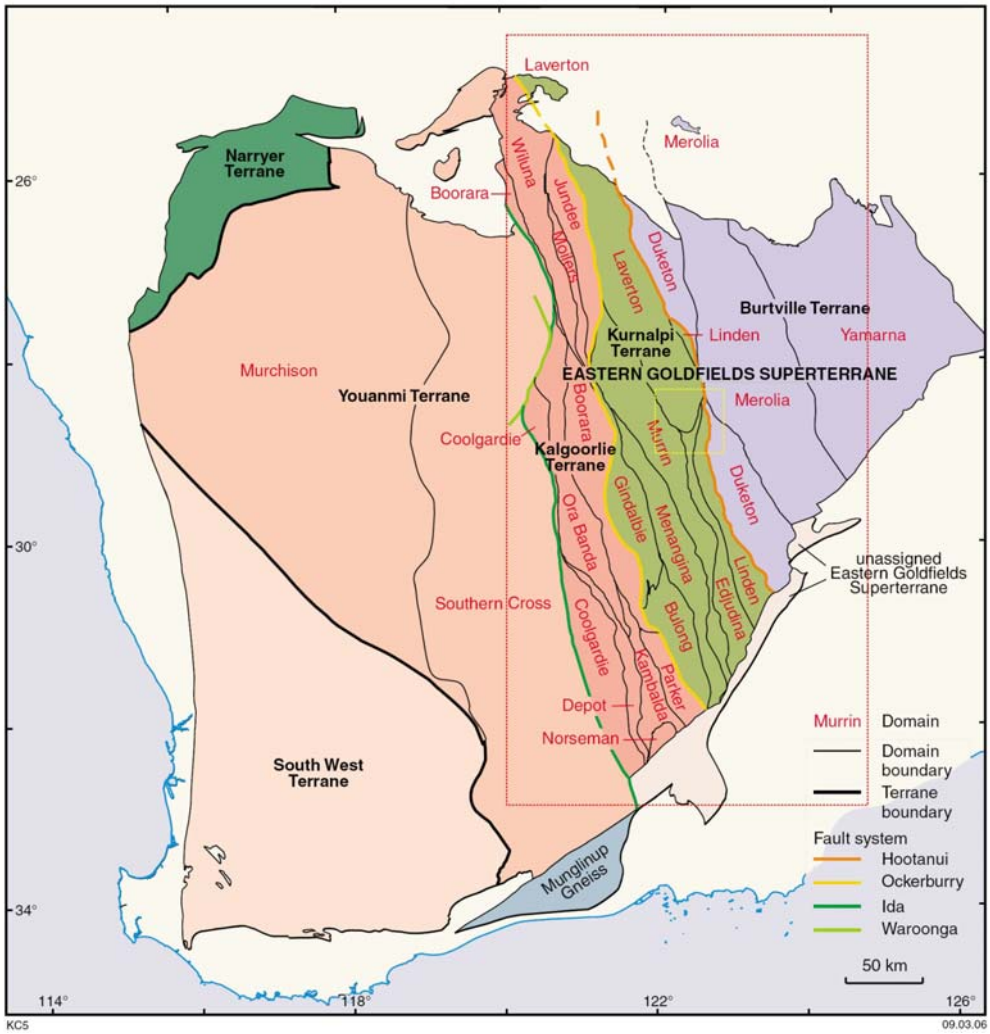

Figure 1: Location map of the study area (red box) and the subdomain of Laverton (yellow) box with terranes and domains of the Yilgarn Craton (after Cassidy et al., 2006).

Data sources

Topographic data were sourced via the online GADDS facility (Geophysical Archive Data Delivery System, available on http://www.geoscience.gov.au). This service provides data from the Geodata 9-second Digital Elevation Model (DEM) of Australia, version 2, published by AUSLIG in 2001. Grid data in a geographic projection (i.e., degrees of longitude and latitude) (GDA94 horizontal datum) with a grid cell size of 0.0025 degrees of longitude and latitude (approximately 250 m) were downloaded and projected to MGA51 (GDA94 horizontal datum). Elevation values are referenced to the Australian Height Datum (AHD). The DEM data are imaged and checked for having any null data within the data set. Null data if present are removed in further processing steps.

Bouguer gravity data (Bouguer density of 2.67 g/cm^3) were sourced from the online GADDS facility. The grid data in geographic projection (GDA94 horizontal datum) from the Gravity Map of Australia published by AGSO in 2001 ("Gravmap01") were obtained

and projected from a grid cell size of 0.008333 degrees (approximately 800 m) to MGA51 (GDA94 horizontal datum). Before carrying out further processing and creating image products, these data were merged with various company supplied grids to produce a higher resolution grid.

Magnetic data were primarily sourced via the online GADDS facility. The Grid data with a cell size of 0.0025 degrees (approximately 250 m) from the Magnetic Anomaly Map of Australia published by Geoscience Australia in 2004 ("Magmap04") were obtained and projected to MGA51 (GDA94 horizontal datum). Before carrying out multi-scale edge detection processing and creating image products, these data were merged with various company supplied grids to produce a higher resolution grid.

In the following we will discuss the processing, synthesis and interpretation of gravity and magnetic data in both regional context and in comparatively smaller regions of EYC.

Processing and qualitative interpretation of Bouguer gravity and magnetic data over the EYC

Qualitative interpretation of appropriately processed gravity or aeromagnetic images is very popular in the geosciences because the simple response functions of mass density or magnetization sources allow the user to intuitively infer information about the horizontal extent of discrete source bodies from the images (e.g., Gunn et al., 1997). These sources are often related to geological units. Examples of the images used in this fashion are gradient maps, upward or downward continued fields, reduced-to-the-pole (RTP) or reduced-to-the equator (RTE) fields, and pseudo-gravity images of magnetic data (e.g., Milligan and Gunn, 1997) etc. Note that some of the processing methods as mentioned above not only enhance the discriminatory power to identify source bodies from the anomaly but become aids for anomaly synthesis also. In the following we discuss various processing steps in the synthesis of Bouguer gravity and total intensity airborne magnetic data over EYC

Image Compilation

The first stage of processing potential field data which are pre-processed with necessary corrections is to distribute the data in an appropriate grid. The grid data are then used for digital processing, image compilations and contrast enhancements etc. There are two categories of digital processing the potential field data (Milligan et al., 2003). For example, one of the categories use the properties of potential field data, such as pole reduction for total magnetic intensity (TMI) data, computing gradients of potential fields etc., while other categories deal with the transformation of potential field data in different domains by using general filtering, image decomposition etc. The second categories of processing examples include spectral analyses, computation of analytical signal, multilevel image decomposition ("Worms") etc. The image contrast enhancement technique with a 3D perspective visualization creates a significant visual impact in identifying geologically important features which otherwise remain subtle, being

attenuated in the dynamic range of surrounding anomaly response. The procedure for image contrast enhancement follows the following steps:

- The grid data are converted to image format aided with a “pseudo-colour” colour composition;
- The resulting colour image is mixed with grey colour shading together with an appropriate sun-angle filter to produce image edge enhancements.

The contrast enhanced images for both Bouguer gravity and total intensity airborne magnetic data over the EYC are displayed with a pseudo-colour scheme and are shown in Figure 2. The left hand image in the panel shows Bouguer gravity data whilst the right hand image shows TMI data. The cell dimensions of the gravity grid were 800 m by 800 m whilst the cell dimensions of the TMI grid were 400 m by 400 m.

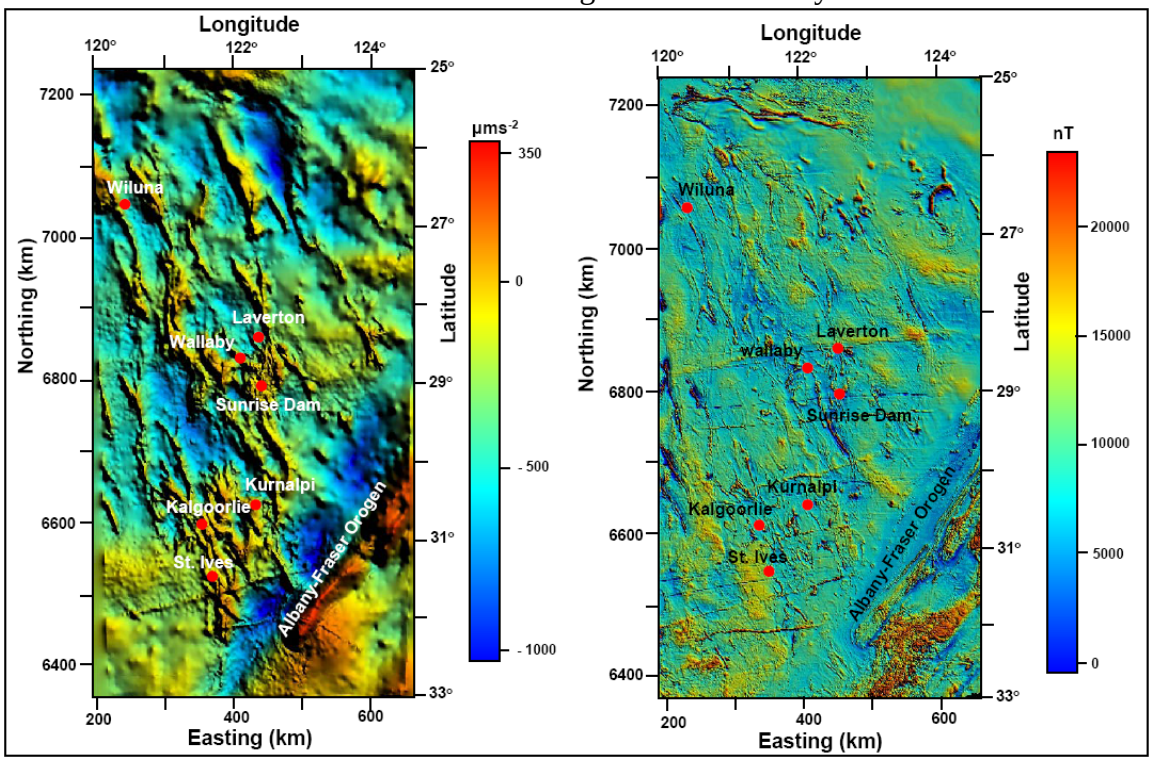

Figure 2. Vertical component simple Bouguer gravity (left) and total magnetic intensity (right) images over the EYC. The maps were prepared using horizontal datum GDA94 and projection MGA51. Existing well known mining areas are indicated with red bullets.

The close observation spacing of the aeromagnetic measurements and the physics of magnetic fields enables finer details to be resolved using magnetic data than is possible using the available gravity data. However, there are caveats to be reckoned with while interpreting qualitatively both gravity and magnetic data through visualization of images. Principally magnetic anomaly sources are dipolar, whereas sources of gravity anomalies are monopolar. In addition, magnetization, the primary cause of magnetic anomalies depends on the distribution of magnetic minerals within rocks in the crust, whereas gravity anomalies are mainly due to variation of bulk property (the density) of the

anomalous sources. Such source characterization has a significant role on the anomaly pattern. In addition, the shape of a magnetic anomaly depends on the inclination of the Earth's geomagnetic field in the area. We address this issue in the following.

Pole Transformation

Direction of magnetization has a profound effect on the shape of the magnetic anomaly, and often leads to a false interpretation. In this context, it is worthwhile to cite the important comment of Roy and Aina (1986) "*A basement high will show up, in total field component measurements, primarily as a magnetic high in high latitudes and a low in low latitudes*". However, in the case of induced magnetization the direction of magnetization at a location is available as an International Geomagnetic Reference Field (IGRF) parameter, the inclination of Earth's geomagnetic field. Note that IGRF parameters vary both spatially and temporally. Once the direction of magnetization is known, its dependency on TMI can be removed either through reduced-to-pole (RTP) or reduced-to-equator (RTE) transformations (Baranov, 1957, 1975). The RTP transformation is preferred over RTE transformation as N-S trending major anomalies are better preserved in RTP than RTE. Further, RTE is suitable in an area of low magnetic latitude. In Figure 3, we present both TMI images with or without RTP transformation for the purpose of comparison. Note that the RTP transformation transforms the shape of some major anomalies into more symmetric shapes.

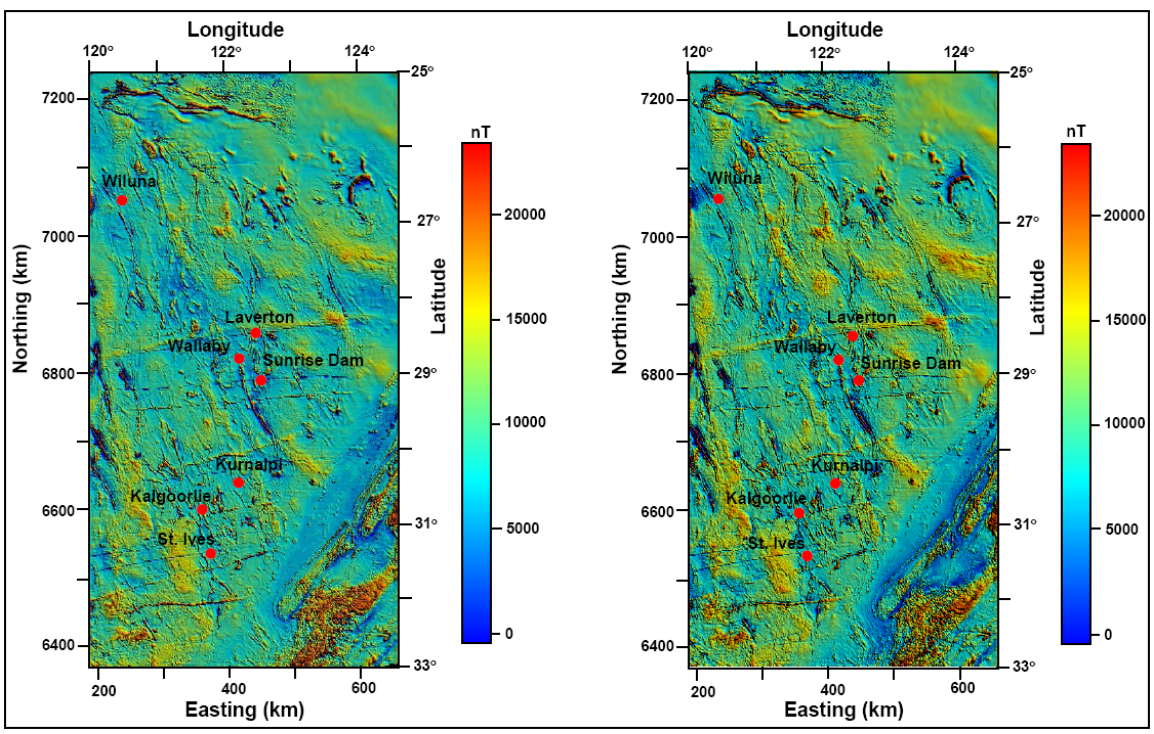

Figure 3. Total magnetic intensity without reduced-to-pole transformed (left) and with reduced-to-pole transformed (right) images over the EYC. The maps were prepared using horizontal datum GDA94 and projection MGA51. Existing well known mining areas are indicated with red bullets. Note that the reduced-to-pole transformation significantly improves the symmetric nature of the anomalies.

In both the gravity and the RTP transformed TMI images signatures of major geologic features are well illustrated; for example, NE-SW trending Albany-Fraser orogen, N-NW trending lineaments are clearly demonstrated in both the gravity and magnetic images. In addition several E-W trending linear anomalous features (dykes) are also clearly noticeable in both the gravity and magnetic images.

It is nevertheless important to note the following caveats, such as (1) assuming a constant value Earth's geomagnetic field parameters at an area may not be valid if the studied area is large; (2) the presence of remanent magnetization effects the selection of geomagnetic field parameters; (3) numerical instability often arises in RTP transformations especially at low magnetic latitudes causing unsatisfactory results. The remedial measure for the first cause could be dividing a large investigative area into smaller areas which are RTP transformed before being joined to the original large area. The effect of remanent magnetization if present is difficult to remove. Note that strong susceptibility and remanent magnetization exist in the studied area, but such magnetization is mainly restricted to near surface effects due to the presence magnetic mineral maghemite formed during the laterization process (Dentith et al., 1994). These near surface anomaly sources add high frequency components in the measured TMI data. Thus, it is expected that an appropriate filtering to TMI data would remove such remanent effects. The remedy for the third cause needs an appropriate algorithmic design. Fortunately, the third cause does not make much impact in our studied area.

Anomaly enhancement

Additional processing of potential field data, such as vertical gradient, analytical signal, multi-scale edge detection (worm) etc. was carried out. Those processes not only enhanced the major anomalies that are apparent in gravity and magnetic images but helped in delineating some more anomalies, which are otherwise subtle in the gravity and magnetic images attenuated in the dynamic range due to presence of high amplitude anomalies. Those processing steps turn out to be major visual aid in identifying the continuity of individual anomalous features whose anomaly strength and shape becomes variable due to variable depth of burial. In the following sections we discuss those in detail.

Vertical Gradient

The motivation in computing vertical gradient or the first vertical derivative of potential field data is to magnify response of the anomaly feature in the image. This can be envisaged as; in the space domain the magnitude of the gradient of potential field varies inversely with distance with one order higher than that of the original potential field due to a source body. Hence, while viewed in the frequency domain this would indicate the enhancement of magnitude of high frequency components. Generation of vertical gradient thus often portrays as a high-pass filtering of the anomaly data. Usual practice in generating a vertical gradient map of potential field data is using Fourier transformation

technique, which unfortunately often cause noise enhancement (Cooper, 2002) and may affect interpretation significantly with anomaly artefacts. Although not always necessary, a band pass filtering with appropriate selection of cut-off frequency is often required before computing the vertical gradient of the anomaly data. The vertical gradient images of both gravity and RTP transformed TMI data over EYC are shown in Figure 4. Note that the sharpness due to image gradients in both the gravity and the magnetic images are significantly amplified.

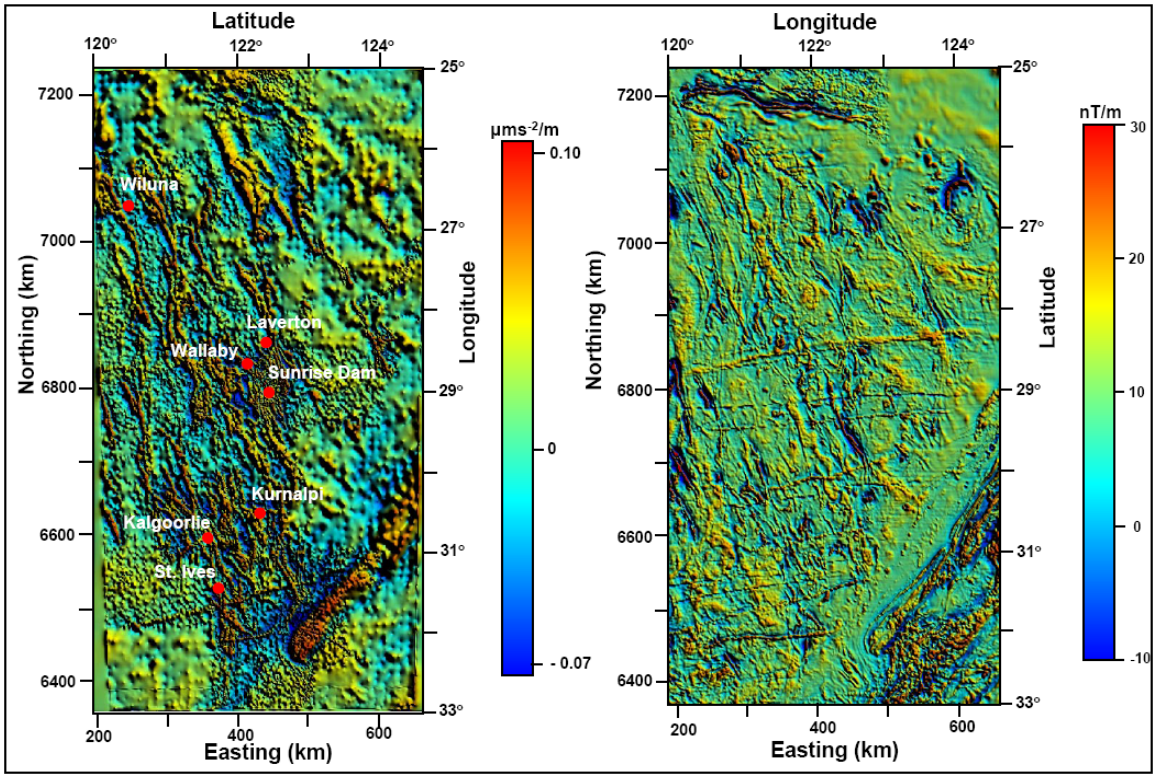

Figure 4. The vertical gradient of Bouguer gravity (left) and reduced-to-pole transformed and band-pass filtered total magnetic intensity (right) images over the EYC. The maps were prepared using horizontal datum GDA94 and projection MGA51. Existing well known mining areas are indicated with red bullets. Note that the vertical gradient computation significantly improves resolution of the images for both Bouguer gravity and TMI data. However, vertical gradient image for TMI resolves more fine structures

While computing vertical gradients of Bouguer gravity data no additional low pass or band pass filtering has been made on the data. However, a band-pass filtering of TMI data were necessary before computing the vertical gradient of it, as frequency content of the magnetic image is more than that of the gravity image and near surface effects are more pronounced in the magnetic image. Thus, the vertical gradient image of magnetic data without any band-pass filtering contains more clutter and possesses difficulty in interpretation. In Figure 5, we present vertical gradient image of reduced-to-pole transformed TMI data with and without band-pass filtered.

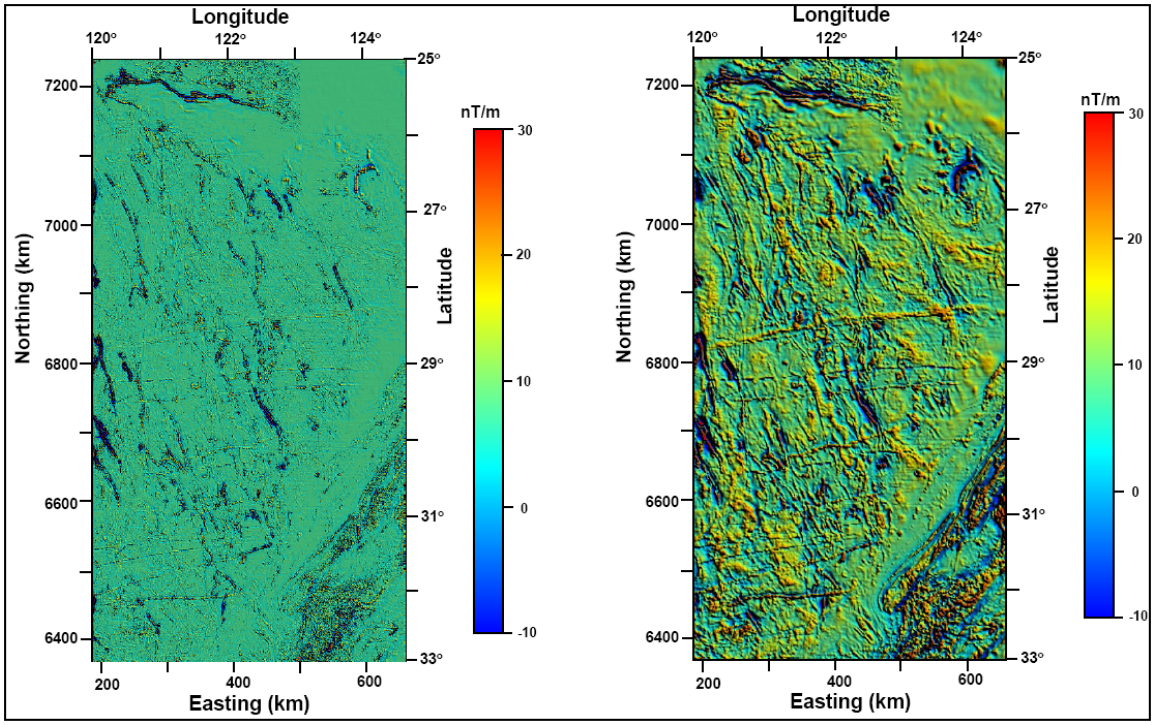

Figure 5. The vertical gradient of reduced-to-pole transformed without (left) and with band-pass filtered total magnetic intensity (right) images over the EYC. The maps were prepared using horizontal datum GDA94 and projection MGA51. Note that the left hand side image of the panel contains clutter due to boost of high frequency noise and has masked significantly the response due to many prominent geological features.

Analytical Signal

The issues related to RTP transformation of TMI data can be overcome by expressing TMI data via *Analytical Signal* (AS). Without going into detail about the definition of the AS we restrict to the idea that an AS of potential field data is such that the amplitude of which is a total gradient of the field and the phase is arctangent of the ratio of vertical gradient to the horizontal gradient of the field, which is also known as tilt derivative (Verduzco et al., 2004). The AS is invariant to the inclination of Earth's geomagnetic field, thus the amplitude of AS would yield positive response over the edges of the source body irrespective of direction of magnetization. However, since the components of AS (amplitude and phase) depend on the value of gradients of the TMI data, AS becomes sensitive to the high frequency part of the signal and the noise as well. Hence, computation of AS be preceded with low pass filtering to suppress high frequency noise effect. In the Figure 6 we present both amplitude and tilt derivative of the AS of TMI data over EYC.

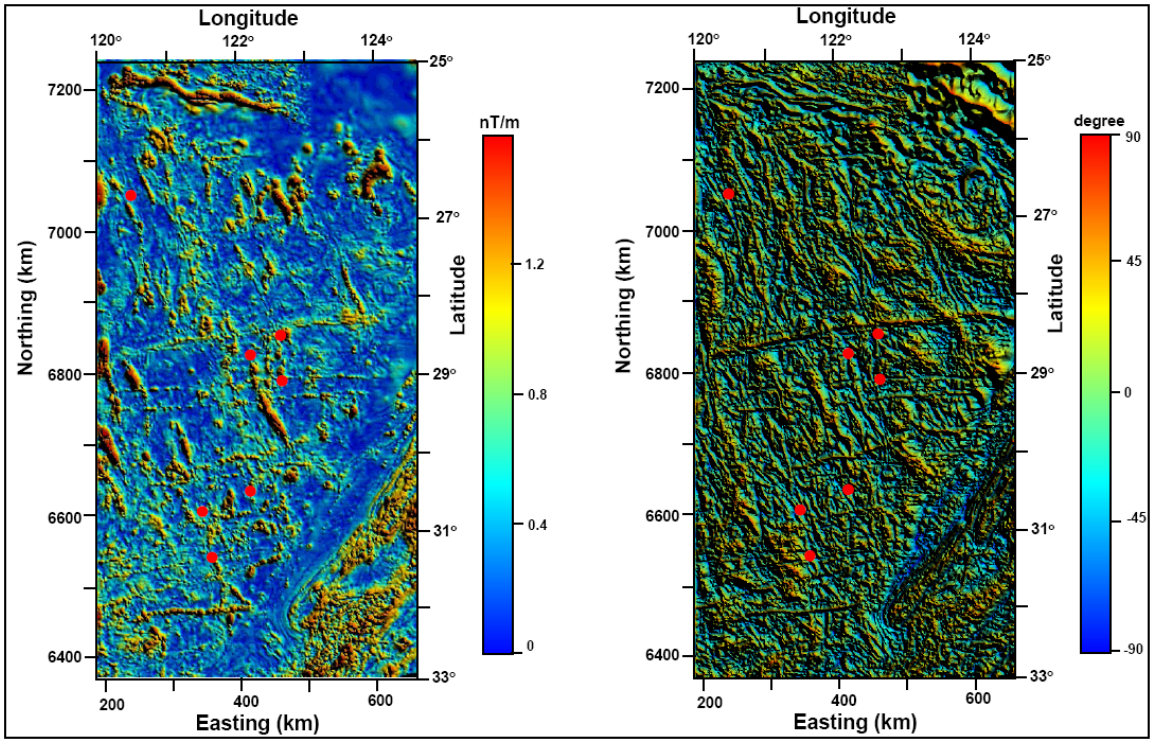

Figure 6. The images of amplitude (left) and tilt derivative (right) of Analytical Signal of TMI data. Note that TMI data is upward continued to a height of 2 km before computing Analytical Signal of the data. This was necessary as Analytical Signal enhances resolution of the image at expense of boosting high frequency noise and unwanted near surface effects. Note that while the strength of Analytical Signal correlates strongly with the magnitude of the anomaly, the phase on the other hand correlates with inverse of depth. Hence, shallow features are likely to be strong in tilt derivative image. The maps were prepared using horizontal datum GDA94 and projection MGA51.

Note that in the above Figure 6, the TMI data has been upward continued to a 2 km height to remove high frequency part before AS computation is carried out. It is important to note that while magnitude of analytical signal closely related to the amplitude of TMI anomaly, the magnitude of tilt-angle derivative is controlled more by the reciprocal of depth of the source body. Hence, the image of tilt-angle derivative would give an idea qualitatively about the depth of the source body.

Multi-scale Edge Detection

Multi-scale edge detection also known as worms has emerged as a popular technique for qualitative interpretation of potential field data (e.g., Jaques and Milligan, 2004; Bierlein et al., 2006; Blenkinsop et al., 2007, Edmiston et al., 2007). This technique is based on the identification of points of maximum horizontal gradient of the fields. Modelling studies with bodies of both regular and irregular shape (Grant and West, 1965; Geldert et al., 1966; Telford et al., 1990) has revealed that, with noiseless data, the points of “local maxima of absolute value of gradient” (LMAG) of an anomaly curve often correspond to the horizontal position of the edge of the body that causes the anomaly. The LMAG of an anomaly curve corresponds to the inflexion point(s) as shown in Figure 7.

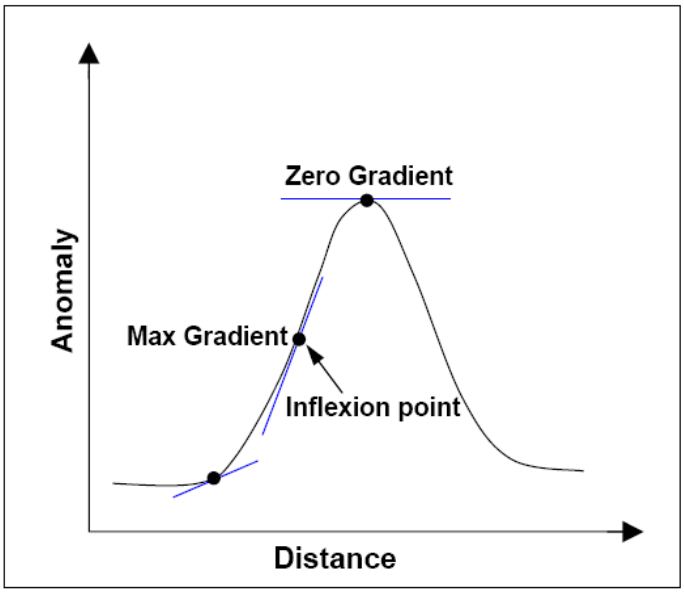

Figure 7. Cartoon of a 1D anomaly (black solid line) with the gradients (blue solid lines) shown at selected points on the curve.

Cordell and Grauch (1982) introduced the concept of generating 'worms' from a potential field anomaly map. They suggested mapping the trace of local absolute maxima of gradient lines (i.e., ridge lines) from maps of horizontal gradients of appropriately filtered (pseudo-gravity transformed) total magnetic intensity (TMI) data. Blakely and Simpson (1986) improved the technique by implementing an algorithm for automatic determination of 'ridge-lines' from a horizontal gradient maps (Figure 8.). Such 'ridge-lines' are the basis of strings or worms.

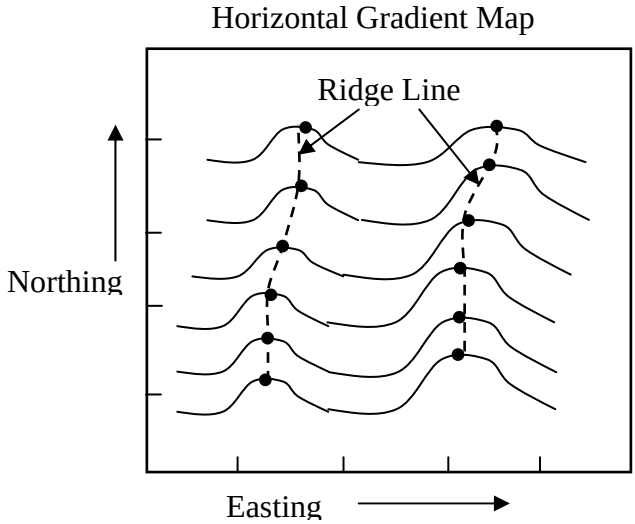

Figure 8. Cartoon showing a series of horizontal gradient profiles. The "ridge-lines" pass through the points that are local maxima of the absolute value of gradients.

Generally, shallow anomalous sources bodies have sharper anomalies above their margins than would be the case for deeper sources. Such generalizations, however, must

be used with caution, as potential field data can be explained by an infinite number of possible source distributions (i.e., by sources that are at different depths or have different spatial extents, etc.).

Sharp anomalies will be most evident when looking at the short spatial wavelength components of potential field data, and conversely, broad anomalies are more strongly represented in the long wavelength components of the data. So called "multi-scale edges" can be derived by altering the spectrum of wavelengths present in potential field data and extracting the points of LMAG from the modified data sets. Upward continuation by increasing amounts is a common means of progressively attenuating short wavelength contributions to the data. Continuation can be achieved using either Fourier-transform or wavelet-transform methods. Hornby et al. (1999) describe a wavelet based edge detection technique. Milligan (2004) has used Fourier transform methods to achieve the same outcome. The latter method has been implemented in the Intrepid™ commercial software package.

We used Milligan's (2004) algorithm and IDL–based codes to generate both gravity and magnetic worms. This involved the following steps:

- Generate multiple data sets employing increasing amounts of upward continuation.
- Starting from an initial continuation distance equal to the grid size, each successive continuation height is obtained by multiplication of the previous height by a constant scale factor.
- This sequence of heights is continued until the height exceeds a chosen value (e.g., approximately 1/5-th the smallest side of the input grid). Through trial and error, we have found that a scale factor of 1.17 gives reasonable results.
- Compute total horizontal derivatives for each upward continued data set.
- Normalise the total horizontal derivative values at each height by multiplying by a constant equal to the ratio of the current continuation height to the initial continuation height.
- Use a Canny filter to isolate the LMAG points.
- Link the LMAG points into strings.

The results of multi-scale edge detection can be viewed and analysed in a variety of ways, for example as a single 2D image or as vector strings in a 3D visualisation environment such as that provided by GOCAD (e.g., Milligan et al., 2003). In a 3D environment, the strings are shown at an elevation corresponding to the level of upward continuation.

Images of multi-scale worms for the gravity and magnetic data over EYC are presented in Figure 9. Both the gravity and magnetic data were upward continued to a maximum height around 89 km. Variety of anomalous features with both very long to short wavelengths ranges can be seen in the worm images. However, to maintain clarity and to identify major anomaly features we have presented here only those worms related to either deep seated or regional scale structures.

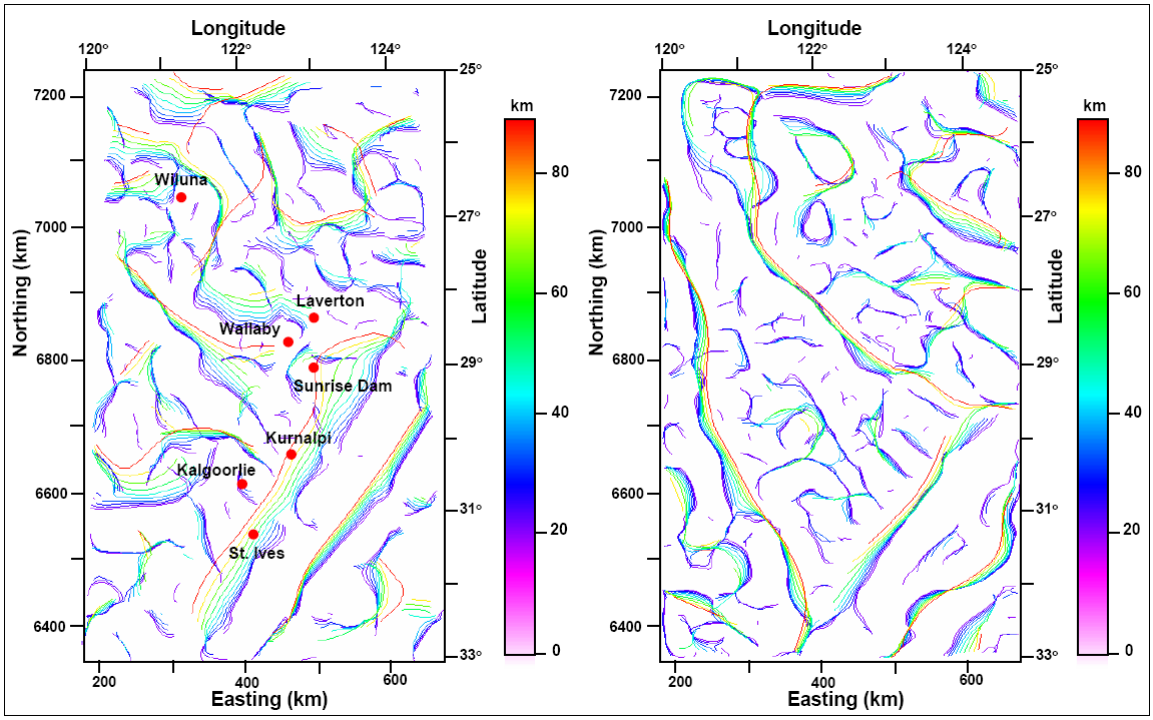

Figure 9. Images of multi-scale worms for gravity data (left) and magnetic data (right). The points of local maxima in anomaly magnitude have been coloured according to the level of upward continuation in kilometres.

3D inversion of Bouguer gravity data over the EYC

Outline

The 3D inverse modelling of potential field data both in regional scale covering an area 404,514 km^2 over EYC and in district scale such as Laverton region covering an area 8000 km^2 were carried out using UBC-GIF GRAV3D (v2.0) and UBC-GIF MAG3D (v3.0) programs. These programs are now most commonly used 3D potential field inversion programs by the mineral exploration industry. Examples of their use can be found in papers by Roy and Clowes (2000), Phillips et al. (2001), Williams et al. (2004), Meixner and Lane (2005), Welford and Hall (2007), and Edmiston et al. (2007). Note that for regional scale inversion over EYC we have only used gravity data. However, we have conducted inverse modelling for both gravity and magnetic data over comparatively smaller area such as at Laverton region. Such preference is made mainly due to logistic purpose.

The strategies of conducting 3D potential field data inversion for regional area and for smaller zone, such as Laverton area are different. There are two aspects in choosing appropriate strategies; such as (1) to fulfil scientific requirement that would address preparation of anomaly data, design of model domain, model resolution or voxet size and (2) logistic constraint, such as computational resources, computational time constraint,

availability of necessary computer software to deal with large scale computational regime. We discuss those strategies in the following.

Inverse modelling of potential field data provides a means of deriving a property model from a set of data observations. Software developed by the University of British Columbia Geophysical Inversion Facility (UBC-GIF) was used for the inverse modelling of potential field data in this study. The software is based on theory and algorithms described by Li and Oldenburg (1996, 1998a). The UBC-GIF 3D potential field inversion algorithm solves linear inverse problem, where a model space is described by a large number of contiguous prismatic cells arranged in honey comb fashion within a large 3D parallelepiped volume that defines the entire model domain. Each of the prismatic cells within the model domain is assigned with specific physical property value, such as density contrast or susceptibility for gravity and magnetic data modelling respectively. Those prismatic cells are also termed as voxells. Smaller size of the voxel would increase the number of their population within the model domain, which in turn increase the resolution of the model space, but at the cost of higher computational burden. To this end we provide a note of caution that the reader must not confused with the model resolution with the term resolution of the model space.

Data Preparation

Preparation of potential field data is an important step of inverse modelling, in that anomaly separation into regional and residual components is a crucial one. The motivation for such exercises is to improve the model resolution by fitting the potential field response due to sources within the domain only, discarding any extraneous effect. However, there is no unique definition for regional and residual anomalies. Nevertheless, an interpreter envisages regional anomalies are due to sources whose extent is large and global in the context of distribution of anomalous sources within the studied region. Hence, a regional anomaly often manifests as a regional trend, which, however is too specific. We have conducted two categories of anomaly separation technique; for inverse modelling the large or regional scale potential field anomaly we have used trend surface analysis to remove the regional effect, while for a smaller region we have used model-based anomaly separation technique.

Regional Removal via Trend Surface

We consider trend surface approach in removing regional component from Bouguer gravity anomaly data at a large regional domain over EYC. Such approach in defining regional component via trend surface analysis is reasonable as our major goal is to delineate geological features which area prominent with their regional trend in the studied region. Selection of the order of trend surface, although somewhat arbitrary is important in defining regional anomaly. We have used graphical method to determine appropriate order of trend surface; in that we have taken several E-W trending profiles and inspect which type of regional best suited. Selection of E-W trending profiles is considered because the major trend of anomaly features are N-NW trending. In the Figure 10 we have presented four such profiles with graphically estimated regional curves.

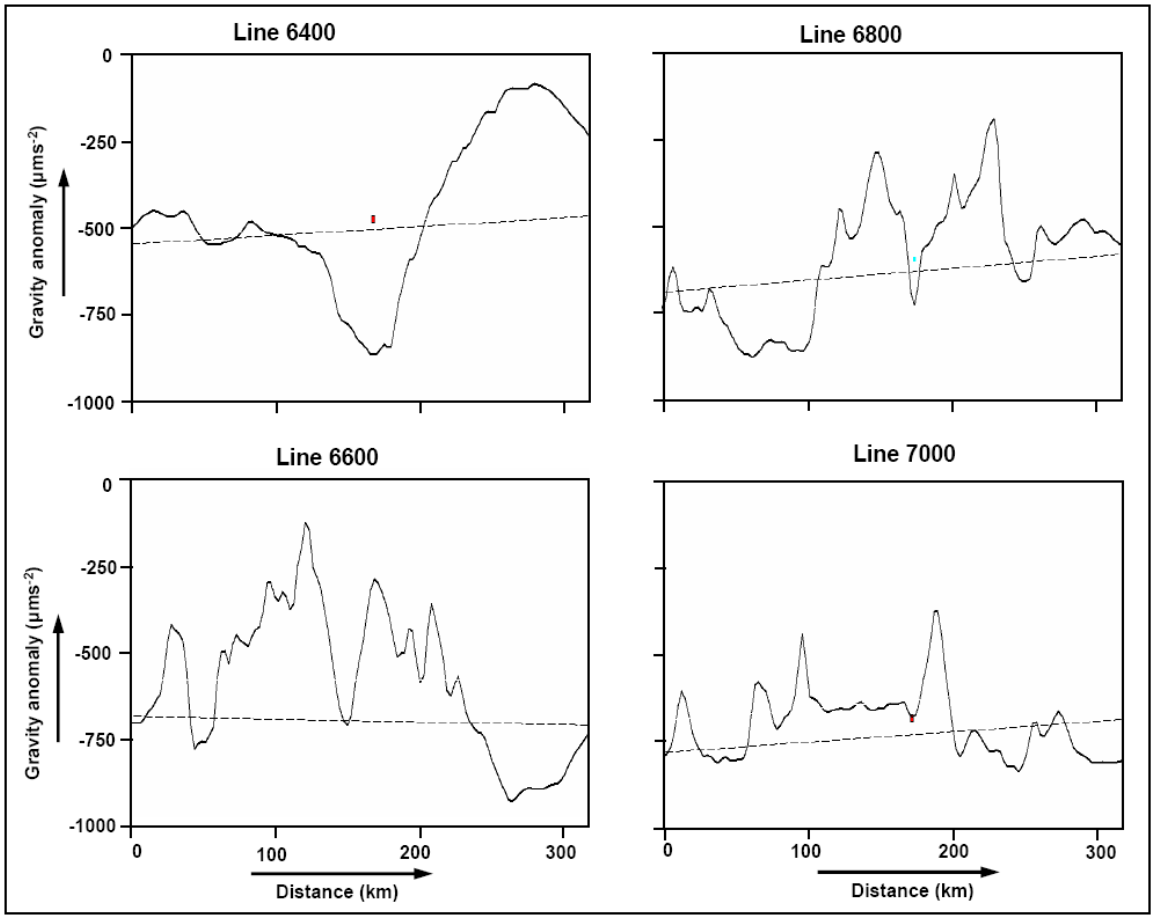

Figure 10. Plot of four gravity profiles taken East-West direction. The line number indicates the profile location at the respective Northings. For example, Line 6600 indicates a East-West profile located at Northing 6600 km in the original gravity Map (Figure 2). Figure 10 clearly demonstrates that the first order trend surface is a reasonable guess for regional anomaly component of the gravity data over EYC.

It is interesting to note that in all four cases simple linear trend is a good approximation for the trend surface. Hence, a first order trend surface is removed from the original gravity anomaly data at large domain over EYC.

Design of Model Domain

In the outset of 3D inversion of potential field data by UBC-GIF software the design of model is crucial. We follow the strategy of Lane and Williams (2004) in designing the model domain. In the following we give a brief outline of the strategy.

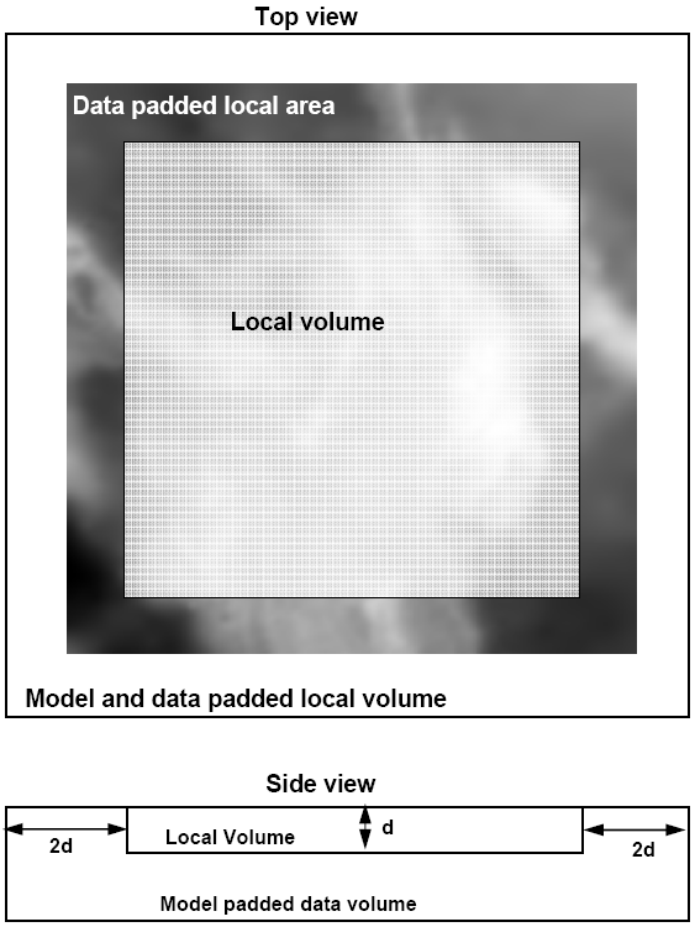

Figure 11. A schematic representation in designing 3D mesh volume. The diagram demonstrates the relative extents of various regions used in 3D inversion procedure. The Figure is adopted from Lane and Williams (2004).

In the Figure 11(a) there are three distinct regions, such as local volume (LV), data padded local area (DPLA) and model and data padded local volume (MDPLV). Note that LV is the only volume that will contain inverted model after inversion run and will be retained; all other volumes/regions which have served to control the edge effect will be removed. The sides of the DPLA region are increased in all four directions by an amount equal to the depth extent of the LV, whereas the sides of the top surface of MDPLV will be increased are increased in all four directions by an amount twice the depth extent of LV. The actual inversion mesh will consider MDPLV volume. Selection of appropriate dimension of the each voxel depends on (1) feasible model resolution with respect to data quality and data sampling, (2) availability of computational resources.

Data Decimation and Collocation

In order to implement UBC-GIF inversion routine on potential field data, it is important that potential field data gets decimated so that the original data grid is diluted to a one, whose cell dimension is same as that of the dimension of the top surface of each voxel.

Such process in turn generates aliasing effect. To remove aliasing effect and to describe the data in same horizontal datum we upward continued the original data to a level same as the largest dimension of the top surface of each voxel. The process of upward continuation acts as an anti-aliasing filter. The data is then decimated so that each data value corresponds to surface location of each voxel. Since topography plays important role in the inversion and since the elevation data in each grid point needs to be the input of UBC-GIF software, we also supply elevation data in each newly generated grid points using Digital Elevation Model (DEM) file of the area. Suites of utility software have been developed to stream line this process to implement UBC-GIF software in an efficient way.

Distributed High Throughput Computing (HTC) via Condor

The 3D inversion of gravity data in a regional scale over the EYC is computationally demanding job, especially when the dimension of the voxels are small. The 3D mesh over the region with voxel size 2 km x 2 km x 2 km results approximately 4.3 million voxels. This possesses a tremendous difficulty in conducting such a large scale inverse modelling in a stand-alone PC within a stipulated period. To overcome such difficulty it is important to adopt a distributed computing scheme. There are two kinds of distributed computing, such as High Performance Computing (HPC) and High Throughput Computing (HTC). Major difference between the HPC over the HTC is the HPC is a tightly coupled distributed system where jobs are running parallel on several computers connected via high-speed network, whereas the HTC system is a loosely coupled distributed system which executes jobs sequentially in a batch mode across several computers connected in a network.

To implement the HPC effectively one needs to develop or modify the existing software (the workhorse) in parallel mode environment using Message Passing Interface (MPI), a communication protocol. Since, there is a little scope in modifying the UBC-GIF software, implementation of the UBC-GIF over the HPC systems is ruled out in the present context. On the other hand, an HTC system does not require modifying existing software, the workhorse. Hence, the HTC system is a preferable alternative to implement 3D gravity inversion on a distributed computing platform. We have used “Condor”, a high-throughput distributed computing system. Condor developed by ‘The University of Wisconsin at Madison’ is a distributed batch computing system and provides a means of opportunistic computing (Thain et al., 2004). The term ‘opportunistic computing’ arises due to Condor’s ability to take advantage of idle machines that they would not otherwise access to.

In order to implement such a distributed computing environment for 3D inversion of the potential field data, it is necessary to split the entire computing domains into several smaller computing domains, where the 3D inversion program will be run in such smaller domains independently. Those decomposed domains are also known as tiles. Each tile is an individual computation unit. The process of tiling the entire large computational domain and the design of each tile dimensions are crucial exercises. A suite of Matlab™ based codes is designed in Geoscience Australia by Dr. Richard Lane, which conducts

several jobs such as generation of tiles with optimal design, preparation of job schedule for HTC system and after a successful completion of the 3D inversion job rearranging and rejoining all tiles to make a seamless 3D inverse model for the entire domain.

Model Appraisal

Results of each inversion were subject to various assessments. Inversion log files were viewed to ensure that the inversion program had terminated in a normal fashion and that an appropriate level of data misfit had been achieved. Assuming an uncertainty related to Gaussian random noise, the achieved misfit is expected to have a magnitude approximately equal to the number of input observations. Such measure is parameterised in statistical sense as chi-square goodness of fit. Images of data misfit (i.e., the difference between observed and predicted data), normalised misfit (i.e., misfit divided by the supplied uncertainty standard deviation), observed data, and predicted data were produced and assessed. In the Figure 12 we present images of observed data, predicted data and data misfit in one panel

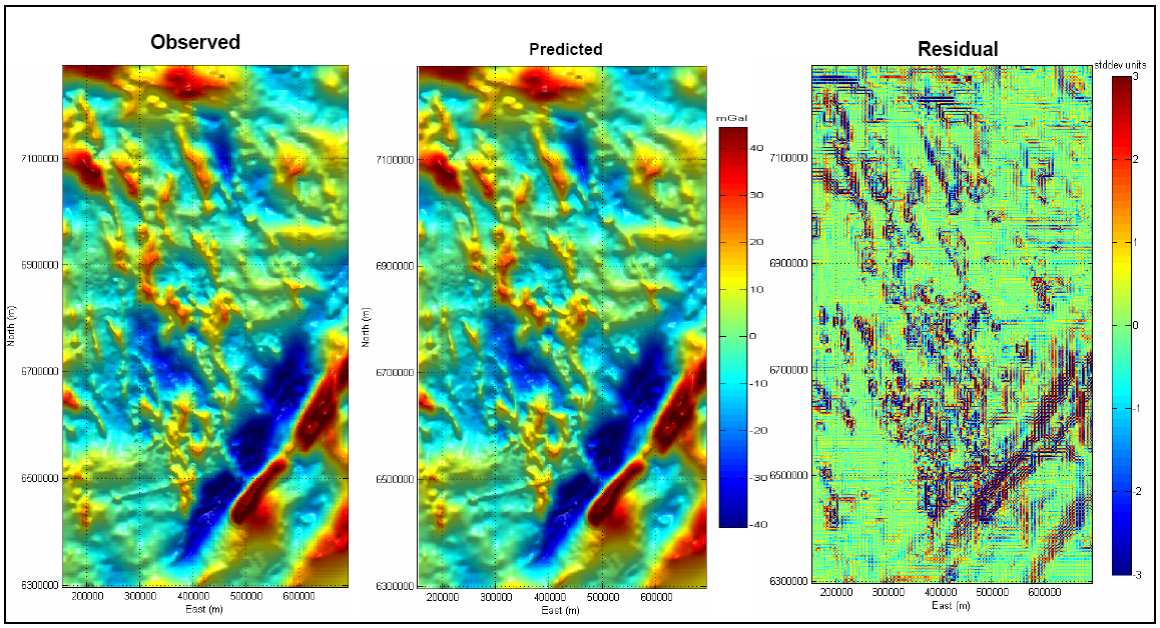

Figure 12. The observed, predicted and residual (observed – predicted) gravity data obtained after 3D inversion are presented in the same panel. The Figures demonstrate a very high quality data fit. The standard deviation of the misfit is extremely small and very low level of correlation exists in the residual map.

Note that the data fit is excellent; the predicted data as expected reproduce the significant anomaly features evident in the observed data with the residual values significantly small. The misfit image is largely dominated by random spatial patterns with only minor amounts of coherent geological signal. A histogram of normalised misfit was generated (Figure 13) and compared with the expected normal distribution (i.e., a mean of zero and standard deviation of 1). The curve traced by the histogram has sharper peak and less width. Note that sharper the peak of the normal distribution curve is lesser the value of

standard deviation around the estimated results. The chi-square goodness of fit also approximates towards 1 indicating a reasonably good fit between the observed data and the predicted one.

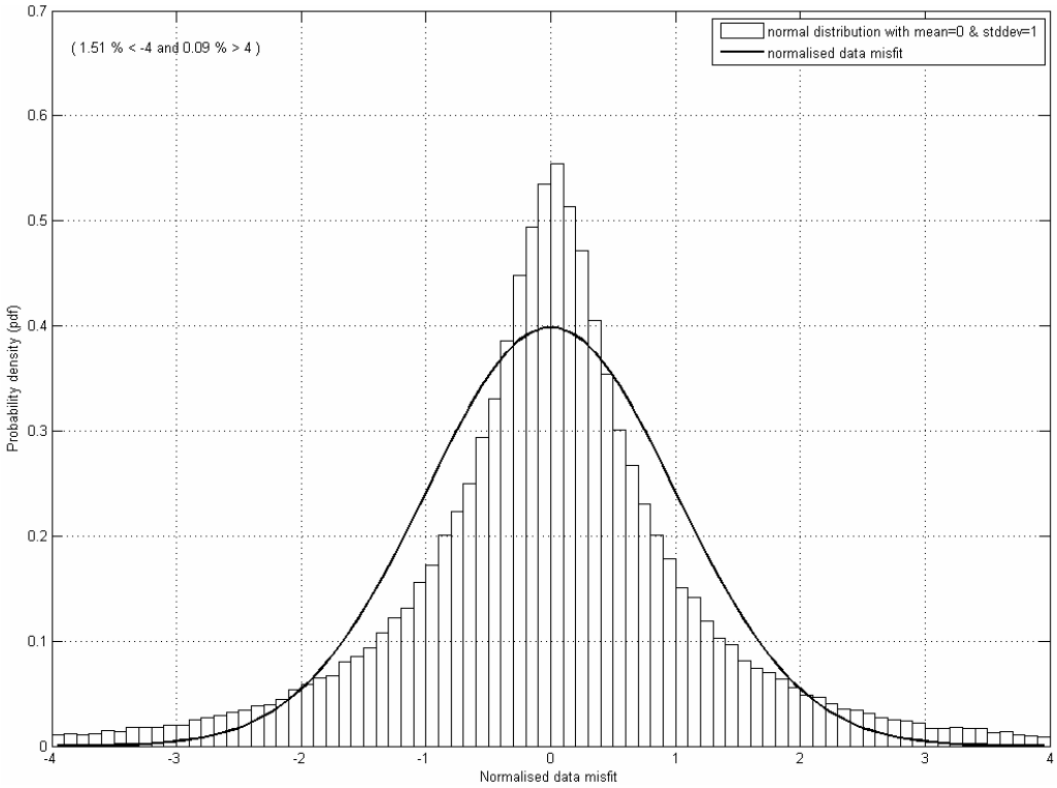

Figure 13. A histogram of normalised misfit and a normal distribution curve with zero mean and unit standard deviation are presented. Note that the curve traced on histogram has shaper peak and smaller width a very high degree of data fit.

In the Figure 14, we present several sections (East-West; North-South; and from the top vertical downwards) of 3D inverted model in one panel for reviewing and comparison purpose. Note that these views of the property model should be dominated by features with a plausible geological origin.

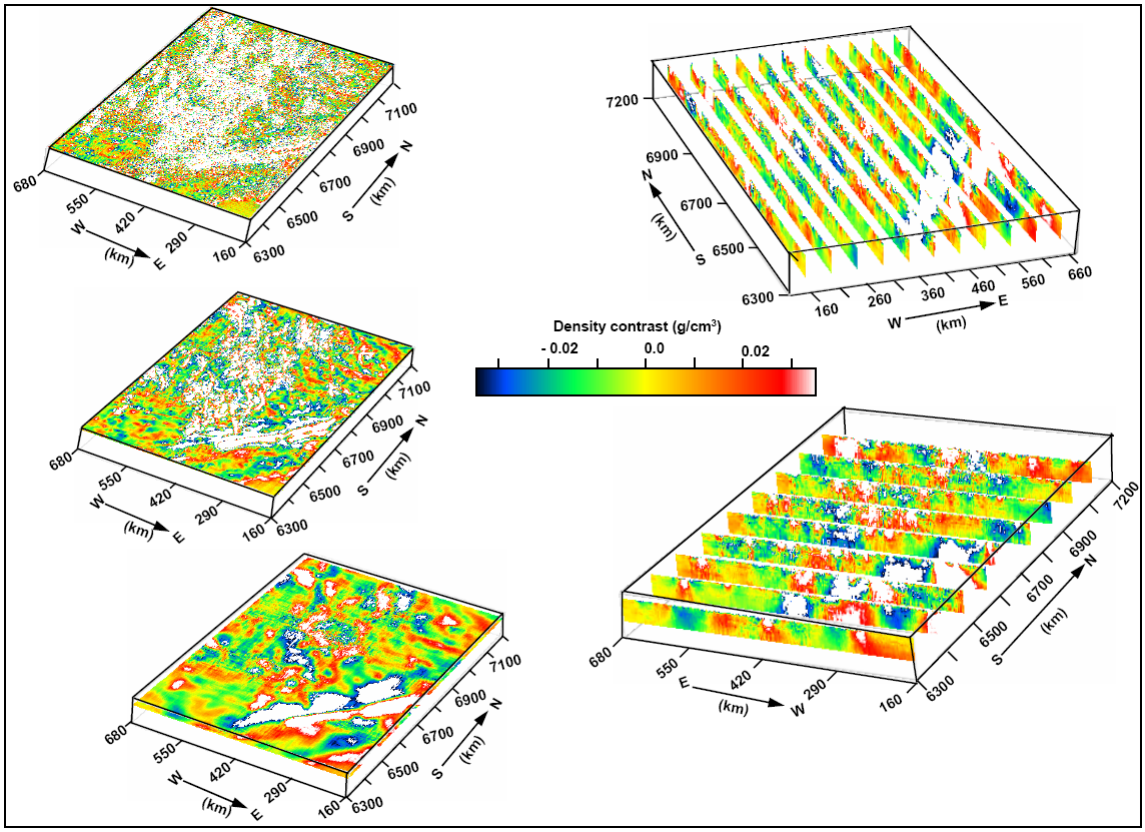

Figure 14. Sections of inverted 3D density contrast model over Eastern Yilgarn Craton (EYC). The slices are taken East-West, North-South and vertical directions. Note that the colour coded model shows the variation of density contrast with respect to the background value of density.

Finally, the property models and model constraints were reviewed with respect to prior geological knowledge to determine what additional insight into the architecture of the region has been obtained.

Gravity and magnetic methods over Laverton region

A detailed study of potential field methods was carried out in the Laverton region over the EYC. The studied region is a district scale with an extent of 80 km x 100 km. The rationales of selecting the Laverton region are viz. (1) the region is the second largest gold mineralized zone over the Yilgarn craton comprising several major mineral deposits, such as Laverton, Wallaby, Sunrise Dam etc; (2) the comprehensive knowledge about architectural framework is necessary to understand the geodynamics of the gold mineralization, which may help in predicting possible mineralized zone(s) over the EYC and (3) availability of high resolution potential field data and reflection seismic data helping in delineating architectural framework of the area by geophysical means. The topographic variation (Figure 15) of this region is moderate to gentle. A moderately rough topography exists in the eastern part of the area, whereas the central and western parts are either flat lying or having relatively gentle topography.

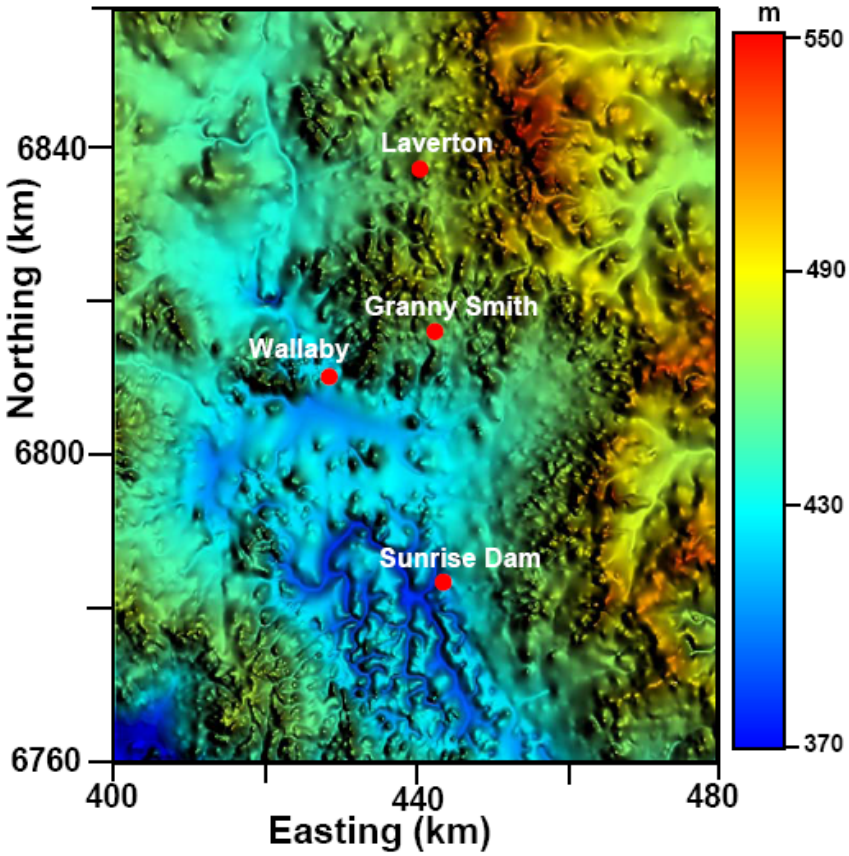

Figure 15. Digital elevation model (DEM) of Laverton region. A moderately rough topography exists at the eastern flank of the area, otherwise the area is more or less flat lying.

The major rock types in this area are gneiss/granitoid, granite, both metamorphosed felsic and ultramafic volcanogenic rocks, greenschists etc (Swagger, 1997). The soild geology map of the area is given in the Figure 16.

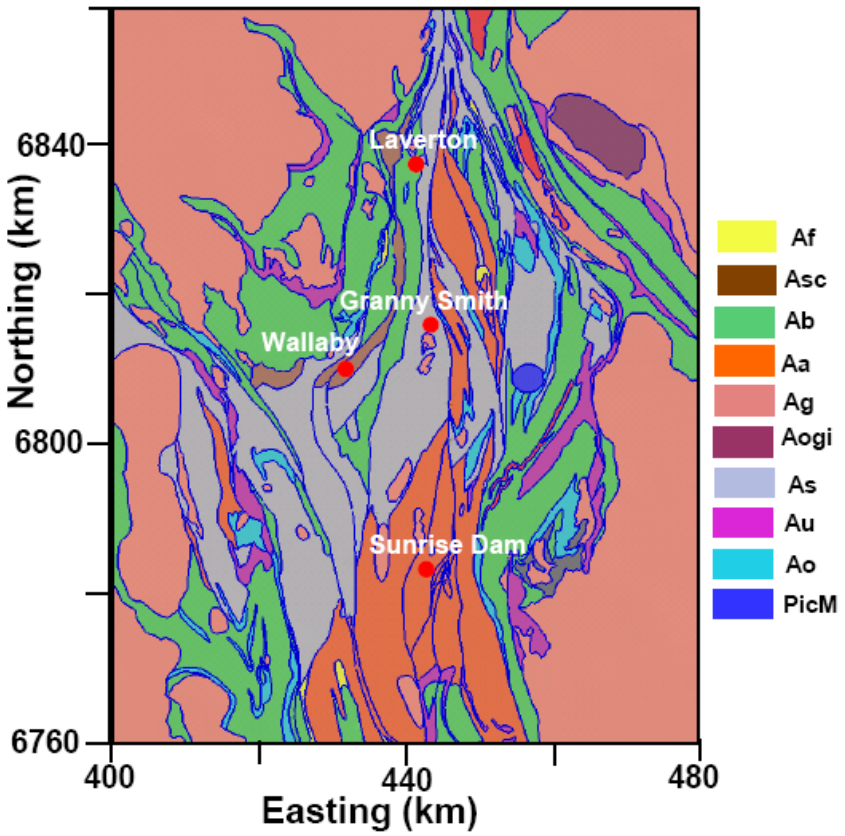

Figure 16. Solid geology map of the Laverton area. One of the major rock types is gneiss or granitoid as a host. Other rocks are greenstone and mafic volcanics etc. (Af: Felsic volcanics; Asc: Conglomerate; Ab: Basalt; Aa: Intrusive intermediate; Ag: Granite; Aogi: Layered ultramafic complex; As: Sediment; Au: Ultramafic; Ao: Dolerite; PicM: Carbonatite

Compilation of Gravity/Magnetic Images and Qualitative Interpretation

As discussed earlier, the compilation of potential field data images with their associated properties and images in various transformation domains play major role in qualitative interpretation through visualisations and correlations with the existing geological knowledge.

Due to availability of high resolution gravity and magnetic data, which although cover a very small portion of the studied area, we have taken a full use of the data by merging with the low resolution gravity data available through GADDS data base using grid merging procedure. Such exercise has improved overall resolution and quality of the potential field data. We used the merged data set for further processing and synthesis purposes. In the Figure 17 we present both Bouguer gravity and reduced-to-pole (RTP) total magnetic intensity (TMI) data.

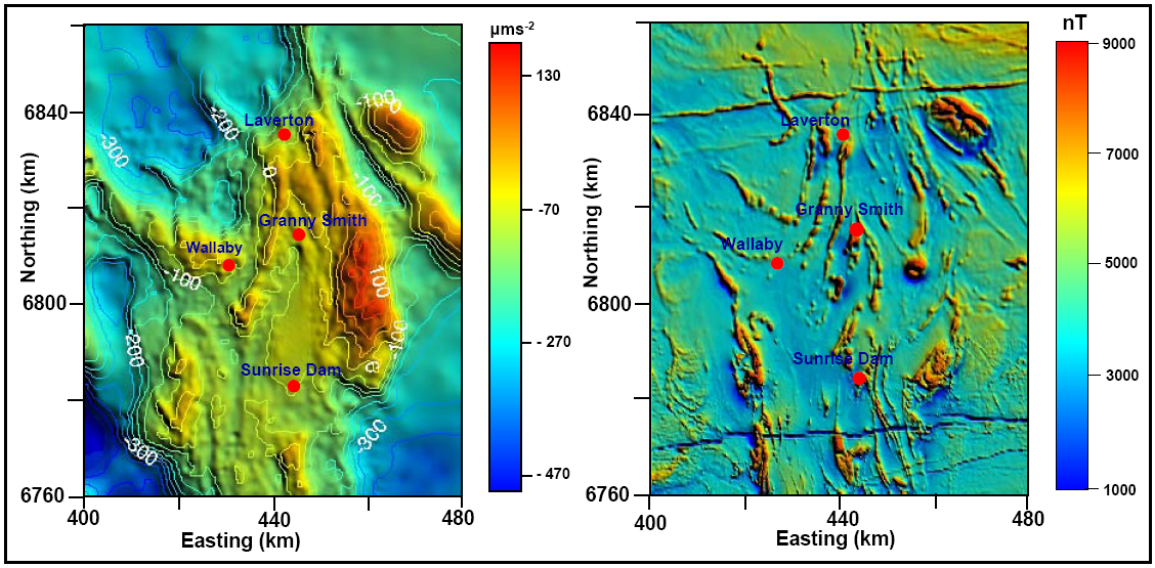

Figure 17. Bouguer gravity and reduced-to-pole transformed total intensity magnetic images at Laverton area. Images area made with respect to Australian datum GDA94 and map projection MGA51. The gravity and magnetic images are made after merging several high resolution but small gravity and magnetic data grids with the gravity and magnetic data grids from GADDS data repository. The cell size of both gravity and magnetic grids are kept at 80 m x 80 m.

The grid merging algorithm does over sampling the available data and generates a grid whose dimension equal to that of the high resolution grid of the area. If the area size of the high resolution data grid is substantially small compared to the low resolution large grid area, then such a very over sampling of data do not necessarily increase the actual resolution, instead it increases the data size unnecessarily. Therefore, resample of data to having a slightly higher grid dimension was carried out. Note that the grid dimension of both the gravity and magnetic data are same 80 m. Although the responses of many major geological features are clearly apparent in both the gravity and magnetic images, the RTP transformed TMI image is sharp and clearly indicates many more geological features.

However, the first vertical both the gravity and magnetic images (Figure 18) reveal many more possible geological features which are otherwise subtle especially in the original gravity image. For example, the E-W trending geological features (dyke) is prominent in magnetic image, but it renders a subtle response in gravity image; however, such features become prominent in first vertical derivative map of both gravity and magnetic data.

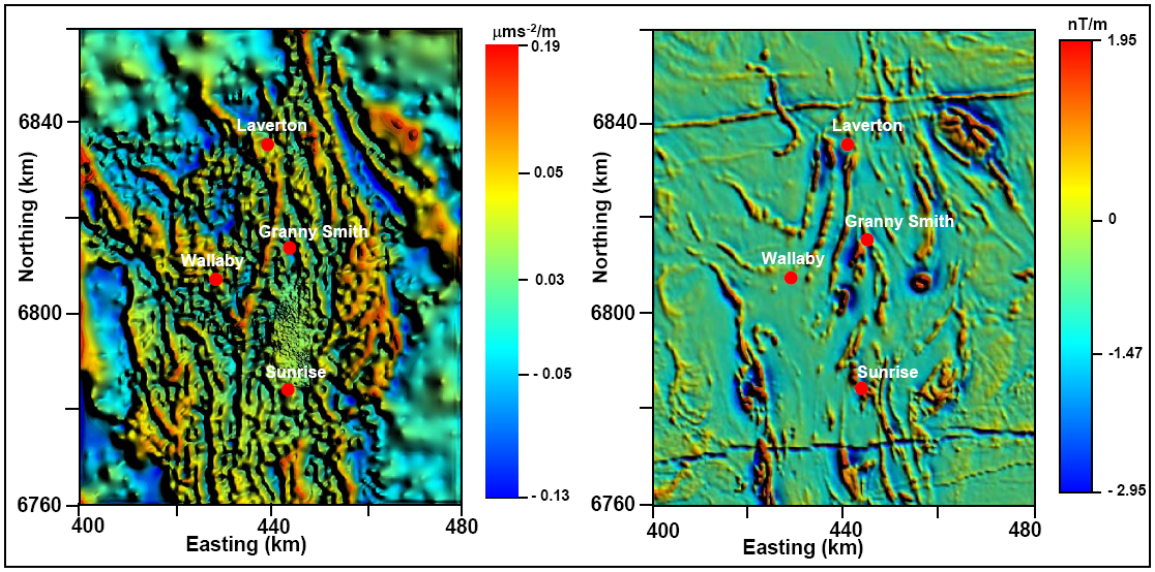

Figure 18. Vertical gradient images for both Bouguer gravity and reduced-to-pole transformed total intensity magnetic data over Laverton region. However in order to improve image quality the magnetic data are filtered with band-pass filter. Note the dramatic improvement of image quality in both gravity and magnetic images.

In addition, analytical signal (AS) of potential field data is another data processing method which is not only very useful being invariant to magnetization direction but also helps in improving the image contrast substantially. We have conducted the AS method on both gravity and magnetic data. In the Figures 19 and 20 we have presented images for the AS and tilt derivatives of gravity and magnetic data respectively.

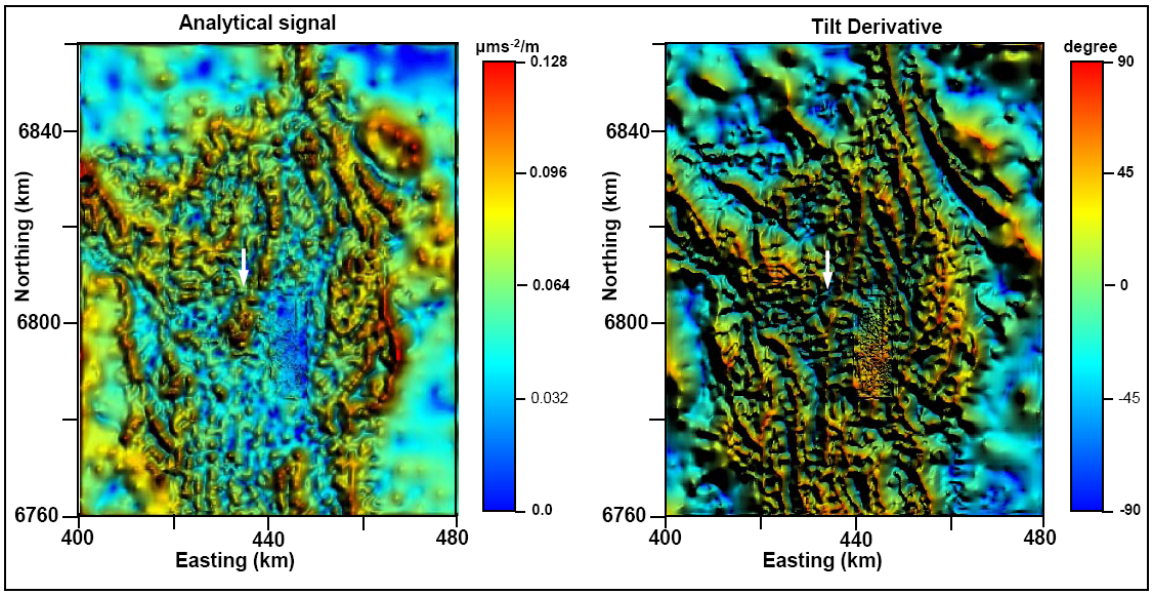

Figure 19. Images of Analytical Signal (AS) and Tilt Derivative (TD) of Bouguer gravity data over Laverton region. Since AS computation is sensitive to high frequency noises the data are low pass filtered

via upward continuation to a level of 500 m. Note that both the AS and TD could reveal a fine structure (white arrow) from the image which is otherwise hidden in the original gravity image.

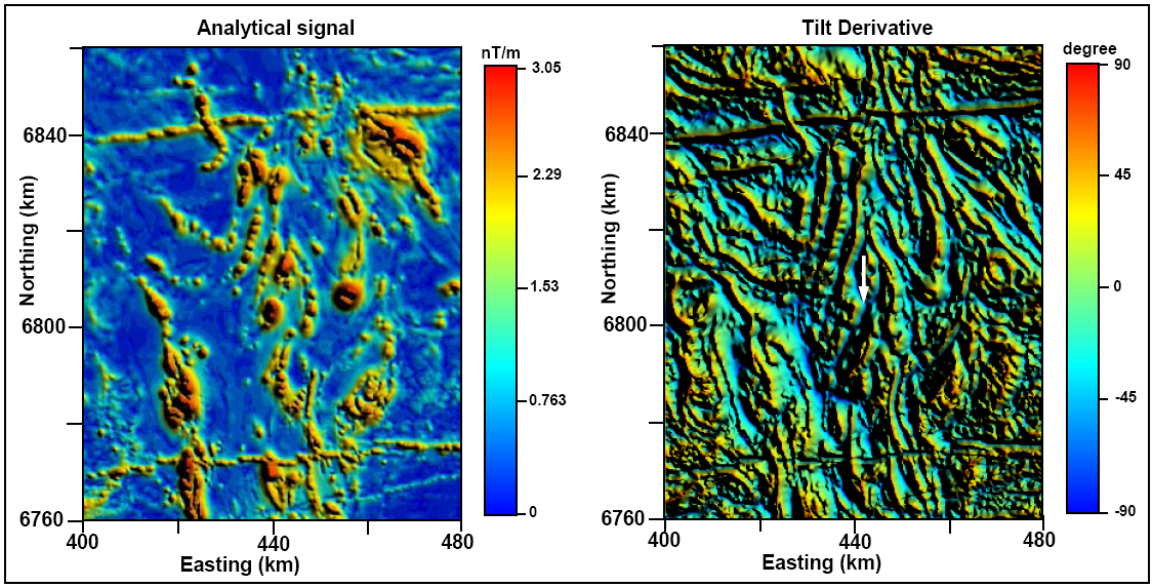

Figure 20. Images of Analytical Signal (AS) and Tilt Derivative (TD) of Bouguer gravity data over Laverton region. Since AS computation is sensitive to high frequency noises the data are low pass filtered via upward continuation to a level of 500 m. Note that the TD can reveal fine structure (white arrow) from the image which is otherwise hidden in the original magnetic image.

Note that in the Figure 19, both AS and tilt derivative reveals E-W trending linear features (please follow the white arrow on the images), whose signature is otherwise subtle in both gravity and TMI images. Such feature is again obvious in tilt derivative image of TMI data (Figure 20). Such feature could possibly be interpreted as a reversely magnetized dyke.

We have also conducted multi-level edge detection or “worming” procedure, the highest continuation level being 15 km. In Figure 21, we present both the gravity and magnetic worm images.

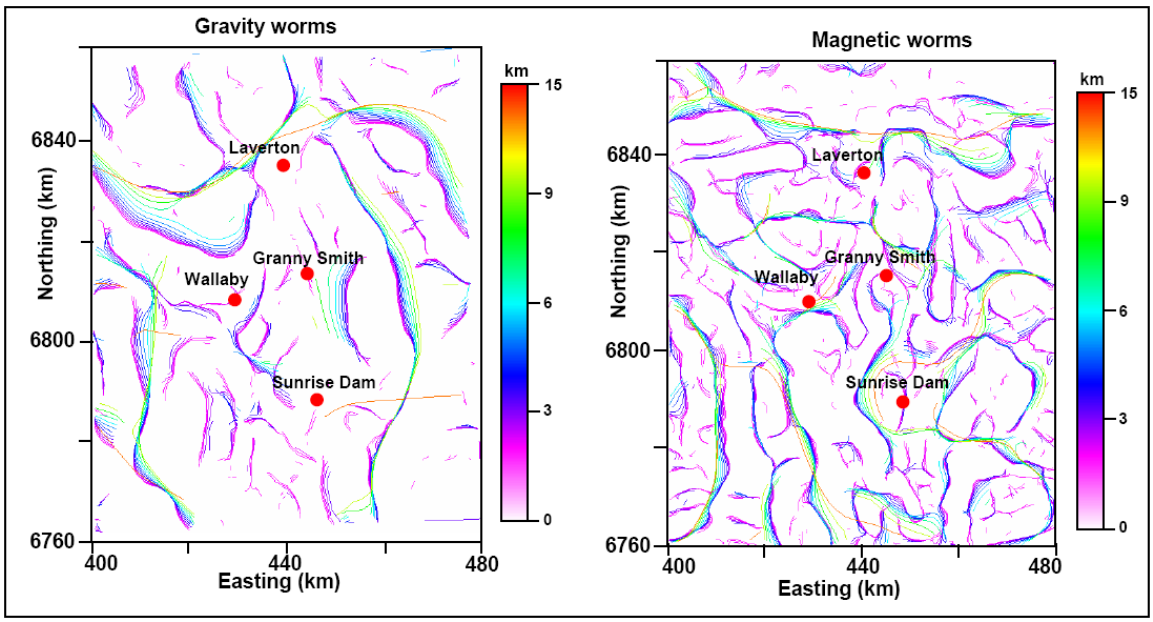

Figure 21. Images of gravity and magnetic worms over Laverton region. The worms are generated for a continuation level u to 15 km. Note that both gravity and magnetic worms indicate several shallow to intermediate depth geological features.

Bothe the gravity and magnetic worms indicate several shallow to upper crustal level anomalous features. Some relatively deep seated structures are also being indicated in the multi-level worm images.

Anomaly separation – a model based technique

Anomaly decomposition of potential field data into both regional and residual components is essential for modelling the potential field data. In the previous section we have mentioned that while decomposing gravity anomaly data in regional scale over the EYC we adopted a linear trend surface as the regional component of gravity anomaly data. Such procedure although is useful for regional scale anomaly interpretation has following drawbacks, such as (1) arbitrariness in order selection, (2) does not reflect true nature of anomaly signature due to large or regional scale anomalous source. We have developed a model based anomaly separation technique, which eliminates above two drawbacks. We have outlined our method with graphical illustration in the following.

The measured gravity and magnetic field data include contributions from sources both within and outside a domain of interest (DOI). We wish to examine only the data that is the result of anomalous properties within our domain of interest. In Figure 22, there are two domains; D1, our domain of interest (DOI), embedded in the larger extended domain D2. There are sources with property contrasts distributed within each domain.

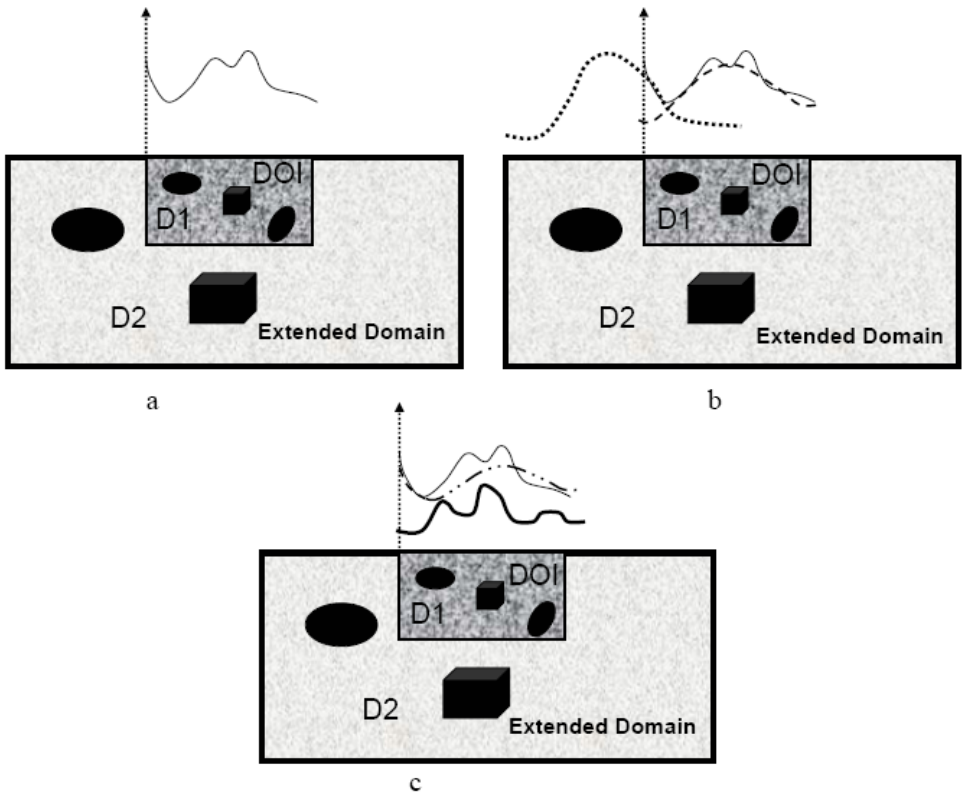

Figure 22. (a) A cartoon depicting source distribution within the domain of interest D1 (dark shaded area) and the extended domain D2 (lightly shaded area) and the measured potential field anomaly at points above D1 due to all sources. (b) The response due to ellipsoidal (dotted line) and cuboidal bodies (broken line) in the extended domain (D2) have been explicitly identified. (c) The total regional response (dash-dot line) due to ellipsoidal and cuboidal bodies in the extended domain D2 and thereby the residual anomaly (thick solid line) due to sources in the DOI have been explicitly identified. These diagrams have been modified from figures supplied by Nick Williams of Geoscience Australia.

Figure 22(a) depicts a measured anomaly response over the surface extension of the DOI. Since the observed potential field anomaly is due to the total response of all possible anomaly sources, the sources outside the DOI will contribute to the measured anomaly on the surface of the DOI. The fields due to these sources outside the DOI are shown in the Figure (b) as the dashed and dotted lines. If we assume that there are no sources within the DOI, then the sum total effect of the anomalies due to sources outside the DOI will be a smooth anomaly (dash-dot line in Figure (c)). This anomaly is termed the "regional anomaly". Subtracting this regional field from the observed field removes the effect of the external sources and produces a residual field which relates only to the sources within the DOI.

In our work, we followed the approach described by Li and Oldenburg (1998b). The regional anomaly due to sources outside the DOI is computed and removed through nested inverse modelling. The basic steps to perform are listed below.

Determine the data extents and mesh parameters required to produce a good result inside the DOI using the nested inversion approach.

- Compile gridded data for a region which is larger than the DOI and completely surrounds it.
- Generate a 3D mesh with an extent larger than the extent of the data coverage. This ensures that a padding zone is available to minimise the introduction of edge artefacts into the property model.
- Remove a first order trend surface from the regional grid data. This is required as the response for the extended domain itself is contaminated by a regional contribution from the remainder of the universe. First order trend surface removal, although arbitrary, has proved a suitable approach when solving for anomalous sources within extended region.
- Some experimentation is required when inverting magnetic data to obtain an appropriate zero level for the de-trended data. A data level that is too high results in a layer of susceptibility across the entire lower part of the model. A data level that is too low results in high susceptibility values within the padding zones around the margins of the model.
- To reduce aliasing and to allow the number of input data to be reduced, data are upward continued to a terrain clearance approximately equal to the horizontal dimensions of the rectangular prisms in the model mesh. At this level of continuation, the data can be safely decimated to a spacing equal to the horizontal dimensions of the mesh elements without introducing additional aliasing. Some experimentation is carried out to determine an appropriate level of uncertainty for the data. The uncertainty values are too low when numerous small artefacts in the property model appear to be related to the noise fraction in the data. The uncertainty values are too high when the data misfit image is seen to contain the coherent spatial response of geological features.
- Invert the regional data to delineate the distribution of density contrasts within the regional mesh volume.
- Set property values for mesh elements within the DOI to zero.
- Compute the forward response due to the source distribution in the remainder (regional) volume at the observation locations that will be used for inversion of the residual data.
- Subtract this response (i.e., the regional anomaly) from the measured anomaly to obtain the residual anomaly.

Although this model-based procedure of anomaly separation is computationally involved, and subject to the normal non-uniqueness of potential field modelling, the technique is objective and enhances resolution of residual anomalies. In Figures 23(a & b) we present the observed, regional and residual anomalies for the gravity and magnetic datasets. Note the significant improvement in resolution of “local source” short spatial wavelength features in the residual anomaly images.

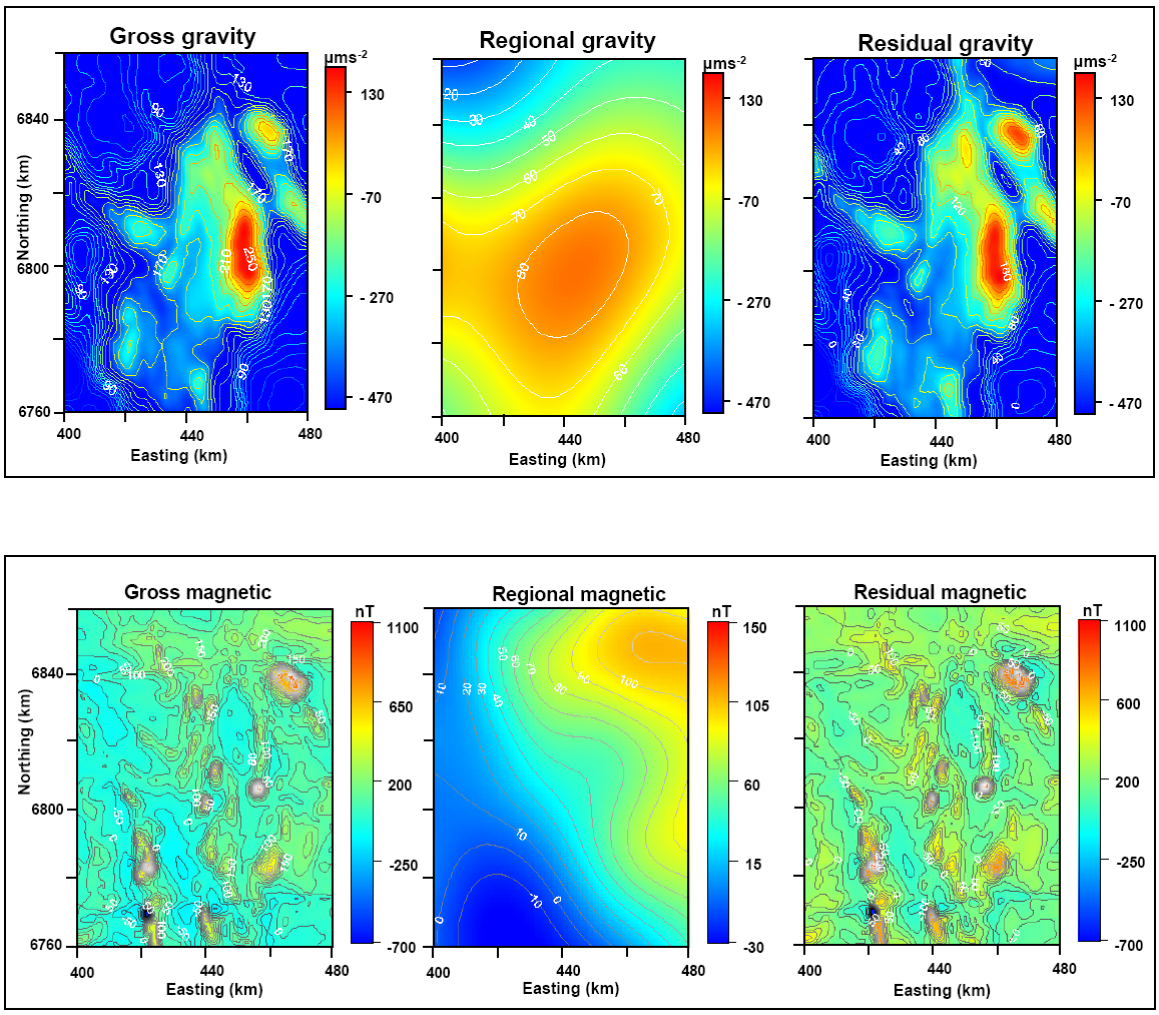

Figure 23. Observed, regional and residual anomaly images. (a) Observed Bouguer gravity anomaly, model-based regional gravity anomaly and residual gravity anomaly images. The contour interval is 20 μms^{-2}. (b) "Observed" reduced-to-the-pole airborne total magnetic intensity (TMI) anomaly, model-based regional RTP TMI anomaly and residual RTP TMI anomaly maps. The contour interval is 50 nT.

3D inversion of Bouguer gravity and magnetic data over the Laverton region

The gravity inversions was carried out as part of a 2 stage process; (1) isolation of a residual component of the relevant potential field through inversion of data from a very large area, and (2) inversion of the residual component to derive a final inversion property model. In conducting the first stage of the process the size of the model domain is at least 8 times larger than that of the actual model domain corresponding to the studied area. The size of each voxel for such a large model domain is also kept very large (5 km x 5 km x 5 km) compared to that of the voxel (dimension: 2 km x 2 km x 2 km) corresponding to the studied area. Smaller voxel size increases the resolution. We will

not discuss inversion methodology here as it is already discussed in the earlier section; instead we will focus on the results and interpretation of inverse model in the following.

3D unconstrained Inversion of gravity/magnetic data

It is important to ensure the quality of the inverse modelling. The first step is to inspect the log file checking whether the achieved misfit value approximates the total number of data samples. We have found that the achieved misfit value corresponding to the inversion of gravity data is 8013 which is close enough to the total number of samples (8000). Similarly, we have observed that the achieved misfit value corresponding to the inversion of magnetic data is 7810, which also closely approximates the total number of samples. Note that the data fitting in both occasions are excellent at least in a statistical sense, although magnetic inversion slightly overestimating. The cases of excellent data fit are also demonstrated in the figures below. FigureFigure 24 and Figure 25 show images of the "observed" data, predicted data and residual misfit from the inversions of residual gravity and magnetic data respectively. These images demonstrate that the inversions converged on solutions (i.e., property models) that could adequately reproduce the main features of the input data.

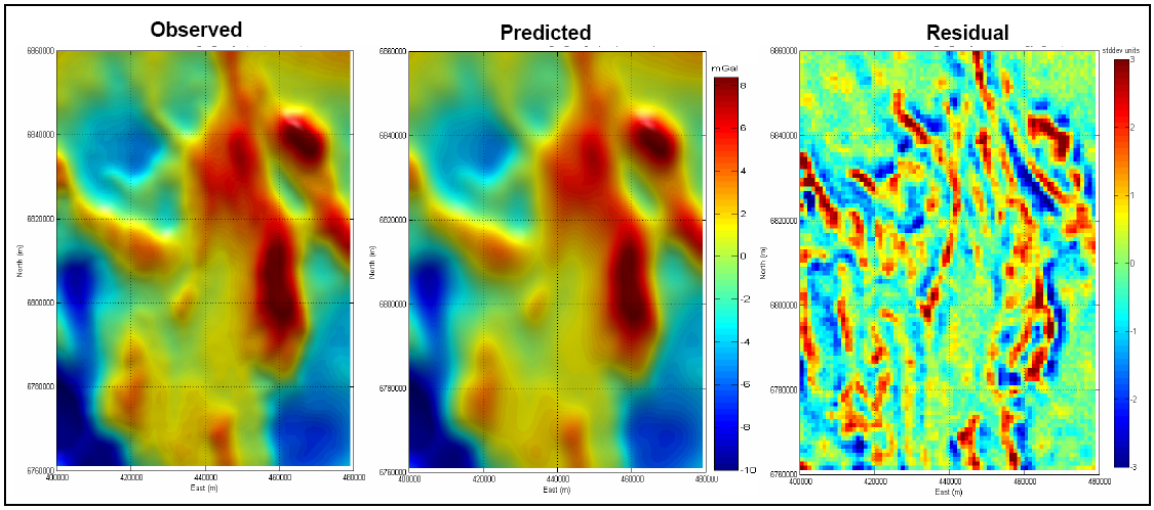

Figure 24. (a) Two dimensional observed (residual) gravity grid data with a grid interval 2 km by 2 km. These data were upward continued to a terrain clearance of 2 km prior to inversion. (b) Predicted gravity data after successful completion of 3D gravity inversion, and (c) normalized data misfit residual. The images demonstrate a generally excellent data fit, with some minor systematic discrepancies between observed and predicted data in regions with strong horizontal gradients.

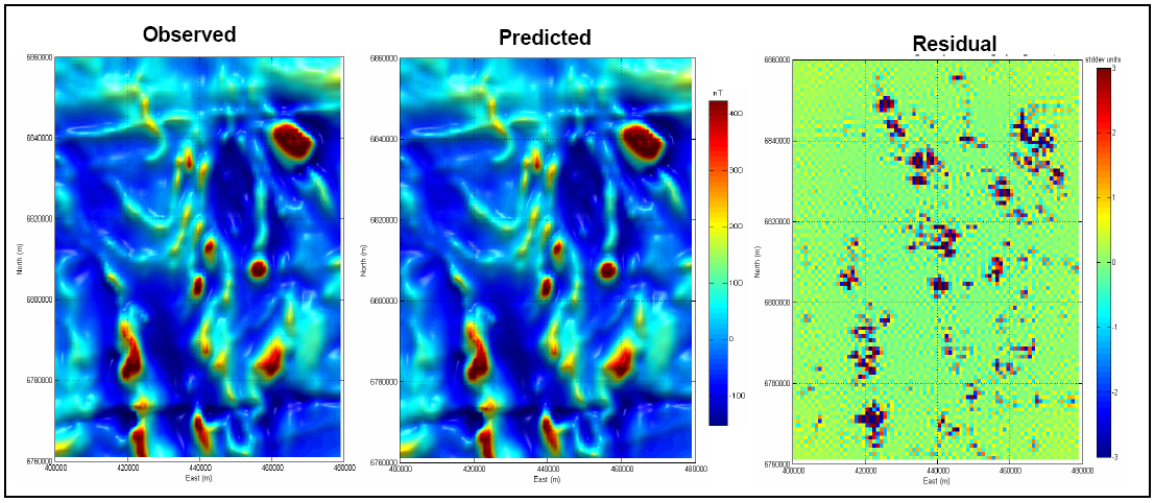

Figure 25 (a) Two dimensional observed (residual) magnetic grid data with a grid interval 2 km by 2 km. These data were upward continued to a terrain clearance of 2 km prior to inversion. (b) Predicted magnetic data after successful completion of 3D magnetic inversion, and (c) normalized data misfit residual. The images demonstrate a good data fit.

Selected views of the density and susceptibility models obtained via inversion of gravity and magnetic data are presented in Figure 26 and Figure 27 respectively. Several west-east and south-north vertical sections together with three representative horizontal slices are shown. Note that the density model sections represent density-contrast values rather than the actual density variation of the subsurface, whereas the susceptibility model represents absolute susceptibility variations of the subsurface. In practice, the Bouguer density (i.e., 2.67 g/cm^3 in this instance) can be considered to be the background density value, and this constant can be added to the density contrast values to obtain a model showing absolute density values.

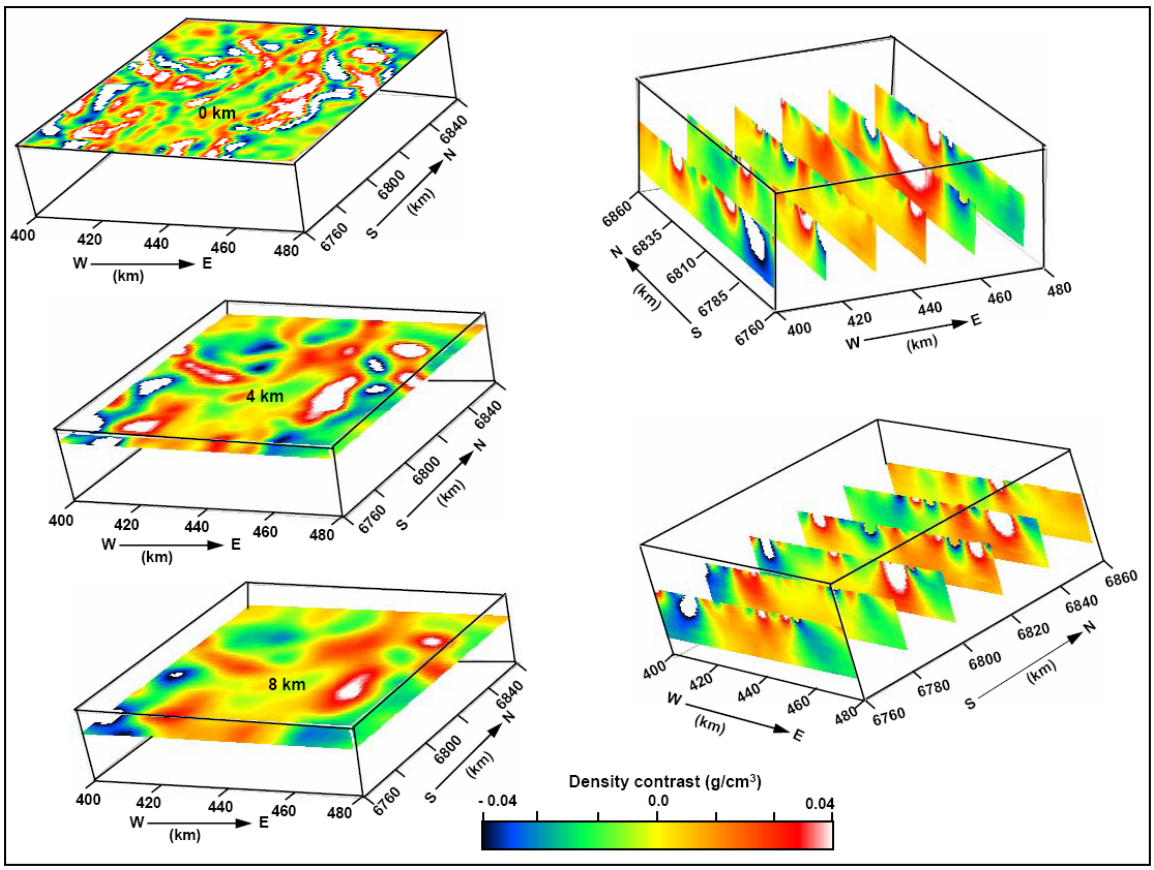

Figure 26. Views of the density-contrast model (in g/cm^3) obtained from 3D inversion of the residual gravity data. The slices are taken in three directions, such as with increasing East, increasing North and increasing depth from the top (0 km) up to 8 km.

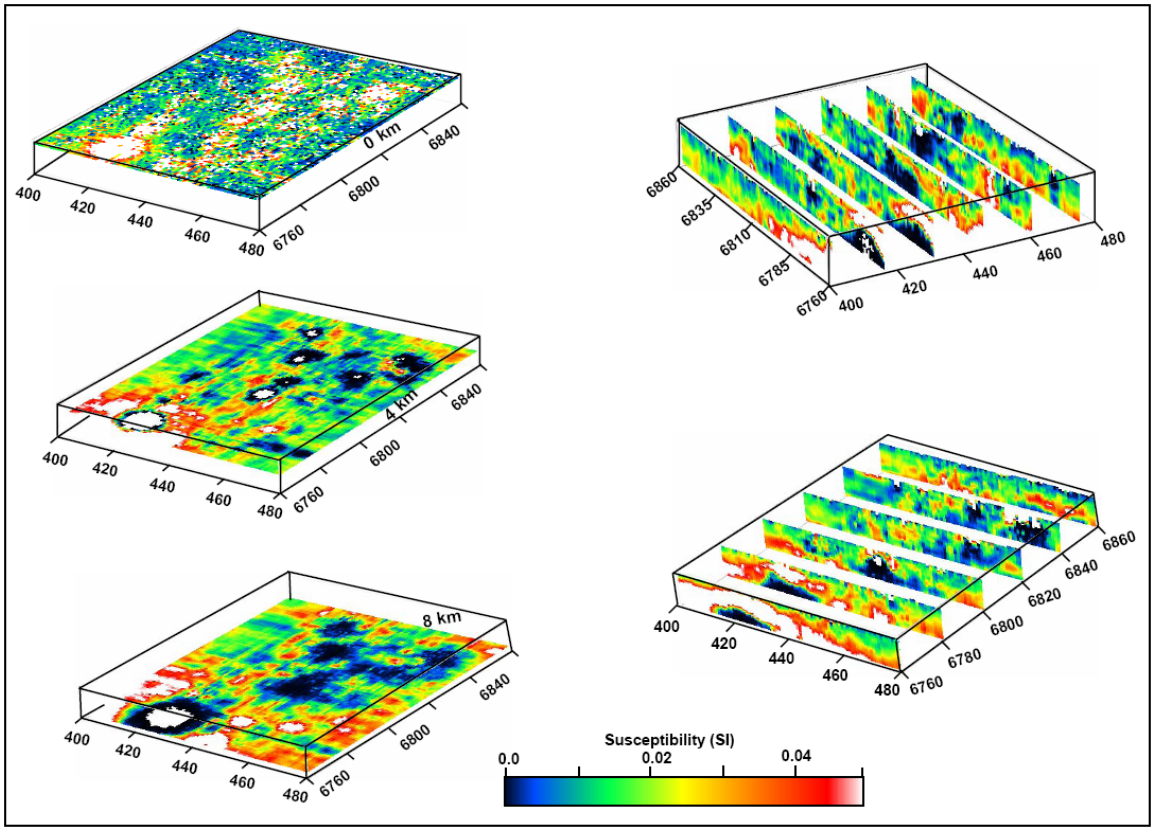

Figure 27 Views of the susceptibility model (in SI) obtained from 3D inversion of residual magnetic data. The slices are taken in three directions, such as with increasing East, increasing North and increasing depth from the top (0 km) up to 8 km.

Forward Modelling Gravity Data

The 3D models obtained via unconstrained inversion of gravity and magnetic data are too coarse. To get a higher resolution model compatible with the known geological model of the area forward modelling of gravity data is essential. However, to conduct a forward modelling exercise two items are essential, viz. (1) *a priori* knowledge of the model and (2) an estimate of the physical property values of the rock type that would describe the model of the area. Note that an *a priori* knowledge of the model is available, through the knowledge of surface geology, limited borehole data and limited seismic sections of the area, whereas, the physical property values such as the measured density values of several rock types in the area are also available in unpublished report (Barlow, 2004). We have conducted 2.5D forward modelling of the gravity data interactively using ModelVision-Pro^{TM} software. In a forward modelling operation for the gravity data several prismatic bodies are drawn and attributed with the appropriate density values of rock type while the background density value is kept constant. For such model a synthetic response is computed and is compared with the observed one. The shape of the prism is altered interactively until a best match between the computed data with the observed one is found. Figure 28 shows several such forward modelling sections of the gravity data.

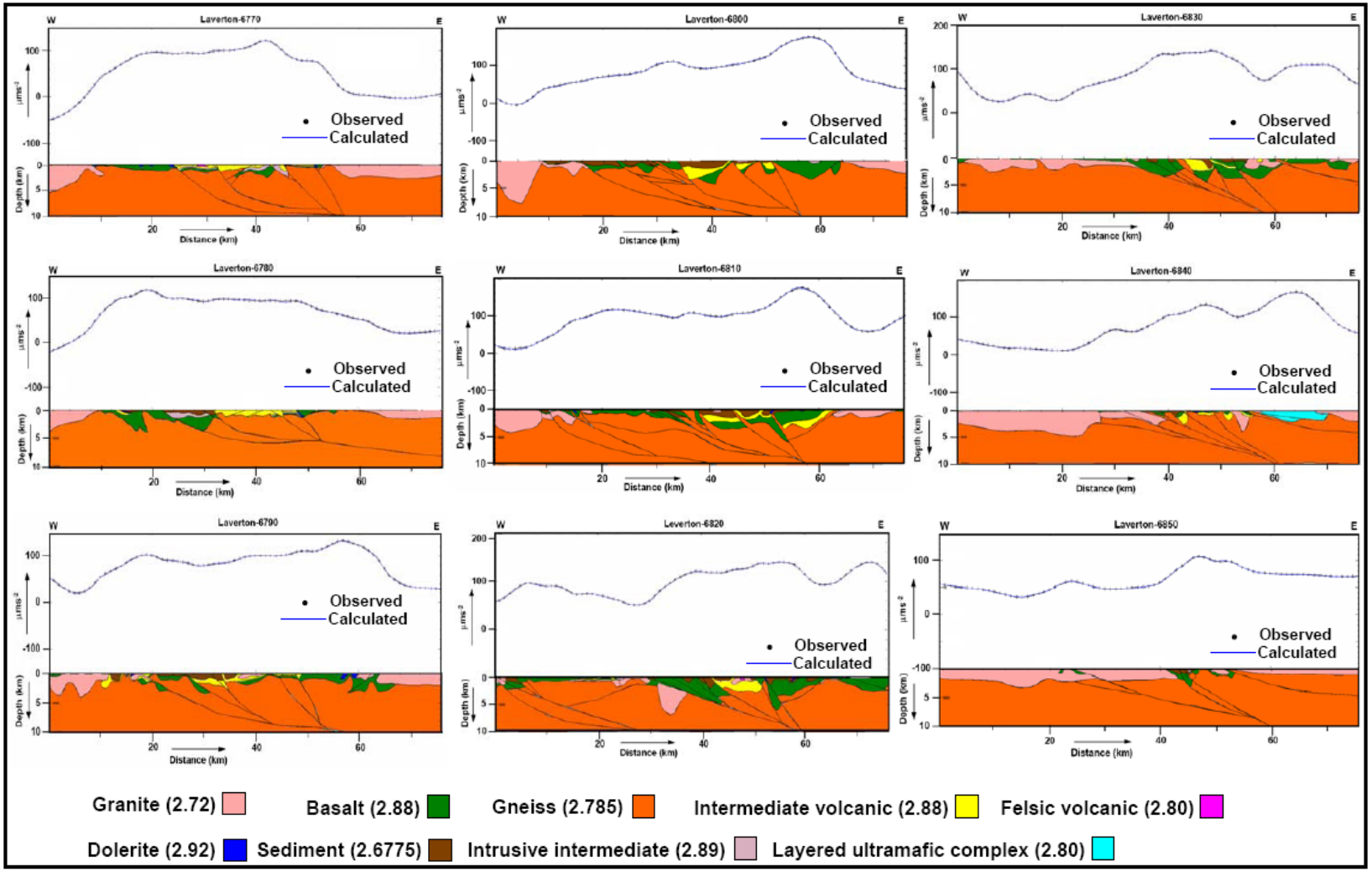

*Figure 28. Geologically controlled sections generated by 2.5D forward modelling of residual Bouguer gravity data over Laverton region. During forward modelling exercise a priori knowledge of the geological settings of the area and the density values of rock types available in the report of the project Y2 of pmd*CRC (Barlow 2004) were used. Excellent data fit between observed data and calculated response are demonstrated in all nine sections.*

An excellent match between the observed and the computed data are found in all nine sections shown here. Such a model, although not unique, is highly constrained with available the geological knowledge in the area.

Discussion

Detailed studies of the application of potential field (gravity and magnetic) methods were carried out in delineating architectural framework of Eastern Yilgarn Craton (EYC) in general (a regional scale) and in Laverton region in particular (a district scale). In our application so potential field methods to provide a thorough geological insights we have used both the data driven and the model driven approaches. In the data driven approach, a major focus is on the generation of high quality images in various data domains, so that it becomes possible to infer at least qualitatively the anomalous features with a geological relevance. The model driven approach on the other hand provides quantitative interpretation of the potential field data and provides estimate of the anomalous sources in all three spatial directions (East-West, North-South and vertically downwards).

To implement model driven applications, we have used 3D linear inversion algorithm (Li and Oldenburg, 1996, 1998a) of gravity and magnetic data using UBC-GIF software and 2.5D forward modelling algorithm. In order to increase the resolving power of the inverted model (at least in smaller region such as in Laverton) we have used a model-based anomaly separation technique to get a best possible residual gravity and magnetic anomalies. The model-based anomaly separation technique is based on the approach of nested inversion described by Li and Oldenburg (1998b). After anomaly separation the residual anomalies corresponding to gravity and magnetic data are inverted with unconstrained inversion technique to generate 3D density and susceptibility models respectively.

However, effective use of UBC-GIF software requires appropriate data preparation and mesh design. A preferred approach for data preparation and mesh design has been developed at Geoscience Australia for use with the UBC-GIF 3D gravity and magnetic inversion programs. The goal has been to minimise the presence of property model artefacts in the user's final volume-of-interest, which is the "Local Volume" as stated in the Appendices 2 and 3. Such unconstrained inversion models are however coarse. Nevertheless, the 2.5D forward modelling of residual gravity anomaly data provides geologically well constrained several vertical sections.

References

Baranov, V., 1957, A new method for interpretation of aero-magnetic maps, Geophysics, 22, 359-383.

Baranov, V., 1975, Potential fields and their transformations in Applied Geophysics: Geopublication Associates, Gebrüder Borntraeger, Berlin and Stuttgart.

Barlow, M., 2004, Density and susceptibility characterization of the Minerie 100,000 geology sheet: Implications for detailed gravity inversion, Unpublished report of Y2 Project, *pmd**CRC.

Barnicoat, A. C., 2007, Mineral systems and exploration science: Linking fundamental controls on ore deposition with exploration process. In: Colin, A. J. (editor): Proceedings of the Ninth Biennial Meeting of the Society for Geology Applied to Mineral Deposits, Dublin, Ireland, August 20-23, 1407-1410.

Blakely, R. J., and Simpson, R. W., 1986, Approximating edges of source bodies from magnetic and gravity anomalies: Geophysics, 51, 1494-1498.

Bierlein, F. P., Murphy, F. C., Weinberg, R. F., Lees, T., 2006, Distribution of orogenic gold deposits in relation to fault zones and gravity gradients: targeting tools applied to the Eastern Goldfields, Yilgarn Craton, Western Australia: Mineralium Deposita, 41, 107-126.

Blenkinsop, T. G., Huddlestone-Holmes, C. R., Foster, D. R. W., Edmiston, M. A., Lepong, M., Mark, G., Austin, J. R., Murphy, F. C., Ford, A., and Rubenach, M. J., 2007, The crustal scale architecture of the Eastern Succession, Mount Isa - The influence of inversion: Precambrian Research (in press).

Cooper, G. R. J., 2003, An improved algorithm for Euler deconvolution of potential field data: The Leading Edge, 1197-1198.

Cordell, L. and Grauch, V. J. S., 1985, Mapping basement magnetization zones from aeromagnetic data in the San Juan basin, New Mexico, in Hinze, W. J., Ed., The utility of regional gravity and magnetic anomaly maps: Expanded Abstract, Ann. Mtg of Soc. Expl. Geoph., 181-197.

Dentith, M. C., Frankcombe, K. F., and Trench, A., 1994, Geophysical signatures of Western Australian mineral deposits: An overview, Exploration Geophysics, 25, 103-160.

Edmiston, M. A., Lepong, P., and Blenkinsop, T.G., 2007, Structure of the Isan Orogeny under cover to the east of the Mount Isa Inlier revealed by multiscale edge analysis and forward and inverse modelling of aeromagnetic data: Precambrian Research (in press).

Eisenlohr, B. N., Gorves, D., Partington, G. A., 1989, Crustal-scale shear zones and their significance to Archaean gold mineralization in Western Australia: Mineralium Deposita, 24, 1-8.

Geldert, L. P., Gill, E. D., and Sharma, B., 1966, Gravity anomalies of two dimensional faults: Geophysics, 31, 372-397.

Grant, F. S. and West, G. F., 1965, Interpretation theory in applied geophysics, McGraw-Hill Book Co. 583p.

Gunn, P. J., Maidment, D., and Milligan, P. R., 1997, Interpreting aeromagnetic data in areas of limited outcrop: AGSO Journal of Australian Geology & Geophysics, 17, 175-185.

Hagemann, S. G., and Cassidy, K. F., 2000, Archaean orogenic load gold deposits. *In*: Hagemann, S.G. and Brown, P.E. (eds.): Gold in 2000 Reviews in Economic Geology, Society of Economic Geology, 13, 9-68.

Hornby, P., Boschetti, F. and Horowitz, F. G., 1999, Analysis of potential field data in the wavelet domain: Geophysical Journal International, 137, 175-196.

Jaques, A.L. and Milligan, P.R., 2004, Patterns and controls on the distribution of diamondiferous intrusions in Australia: Lithos, 77, 783-802.

Lane, R., and Williams, N., 2004, Guide to preparing a smooth model potential field inversion, using UBC-GIF MAGINV3d and GRAV3d software packages, Geoscience Australia Report

Li, Y., and Oldenburg, D.W., 1996, 3D inversion of magnetic data: Geophysics, 61, 394-408.

Li, Y., and Oldenburg, D.W., 1998a, 3D inversion of gravity data: Geophysics, 63, 109-119.

Li, Y., and Oldenburg, D.W., 1998b, Separation of regional and residual magnetic field data: Geophysics, 63, 431-439.

Meixner, A.J., and Lane, R., 2005, 3D inversion of gravity and magnetic data for the Tanami Region: Annual Geoscience Exploration Seminar (AGES) 2005, Record of Abstracts, Northern Territory Geological Survey Record 2005-001.

Milligan, P.R., 2004, Multi-scale analysis of potential field data – Geoscience Australia implementation: Unpublished Technical Report.

Milligan, P.R., and Gunn, P.J., 1997, Enhancement and presentation of airborne geophysical data: AGSO Journal of Australian Geology & Geophysics, 17, 63-75.

Milligan, P.R., Petkovic, P. and Drumond, B. J. (2003) Potential field datasets for the Australian region: their significance in mapping basement architecture: Evolution and Dynamics of Australian Plate, eds., R. R. Hillis and R. D. Muller, Special paper 372, The Geological Society of America, 432p.

Milligan, P.R., Lyons, P., and Direen, N., 2003, Spatial and directional analysis of potential field gradients - new methods to help solve and display three-dimensional crustal architecture: Extended Abstracts, ASEG 16th Geophysical Conference and Exhibition, February 2003, Adelaide.

Phillips, N., Oldenburg, D., Chen, J., Li, Y., and Routh, P., 2001, Cost effectiveness of geophysical inversions in mineral exploration: Applications at San Nicolas: The Leading Edge, 20, 1351-1360.

Roy, A., and Aina, A. O., 1986, Some new magnetic transformations, Geophysical Prospecting, 34, 1219-1232.

Roy, B., and Clowes, R.M., 2000, Seismic and potential-field imaging of the Guichon Creek batholith, British Columbia, Canada, to delineate structures hosting porphyry copper deposits: Geophysics, 65, 1418-1434.

Swagger, C.P., 1997, Tectono-stratigraphy of late Archaean greenstone terranes in southern Eastern Goldfields, Western Australia, Precambrian Research, 83,11-42.

Telford, W.M., Geldert, L.P., and Sheriff, R.E., 1990, Applied Geophysics: 2nd Edition, Cambridge University Press, New York.

Thain, D., Tannenbaum, T., and Livney, M., 2004, Distributed computing in practice: The Condor experience: Concurrency and Computation: Practice and Experience, 17, 323-356.

Verduzco, B., Fairhead, J. D., and Green, C. M., 2004, New insights into magnetic derivatives for structural mapping, The Leading Edge, 23, 116-119.

Welford, J.K., and Hall, J., 2007, Crustal structure of the Newfoundland rifted continental margin from constrained 3-D gravity inversion: Geophysical Journal International, 171, 890-908.

Williams, N.C., Lane, R., and Lyons, P., 2004, Regional constrained 3D inversion of potential field data from the Olympic Cu-Au province, South Australia: Preview, Issue 109, 30-33.